AN EVALUATION SYSTEM FOR MECHANICAL AND ELECTRICAL CHARACTERIZATION OF MEMS DEVICES

Except where reference is made to the work of others, the work described in this thesis is my own or was done in collaboration with my advisory committee. This thesis does not include proprietary or classified information.

Seong Jin Kim

Certificate of Approval:

George T. Flowers
Professor
Mechanical Engineering

Robert N. Dean, Chair
Assistant Professor
Electrical and Computer Engineering

Bogdan M. Wilamowski
Professor
Electrical and Computer Engineering

Thaddeus Roppel
Associate Professor
Electrical and Computer Engineering

George T. Flowers
Dean
Graduate School

AN EVALUATION SYSTEM FOR MECHANICAL AND ELECTRICAL CHARACTERIZATION OF MEMS DEVICES

Seong Jin Kim

A Thesis

Submitted to

the Graduate Faculty of

Auburn University

in Partial Fulfillment of the

Requirements for the

Degree of

Master of Science

Auburn, Alabama
May 9, 2009

AN EVALUATION SYSTEM FOR MECHANICAL AND ELECTRICAL CHARACTERIZATION OF MEMS DEVICES

Seong Jin Kim

Signature of Author

Date of Graduation

VITA

Seong Jin Kim graduated from Joongdong High School in Feburary of 1987 and Yonsei University in August of 1992 with a Bachelor of Science of Electronic Engineering. After graduation, he worked for Halla Engineering and Heavy Industries, Ltd. as an aerospace electrical engineer for five years. He then continued his electrical design career in MilS Engineering Ltd. for six years, and then worked for EO System Co., Ltd. After several projects, he worked on a MEMS uncooled focal plane array (UFPA) detector at EO System Co., Ltd, where he became fascinated with MEMS technology and then decided to pursue graduate work in MEMS fabrication, packaging and testing at Auburn University.

Seong Jin Kim was born to Si-Hwan Kim and Byoung-Won Suh on the 16th of September, 1967 in Seoul, Korea. He married Eun Jung An on September 28, 1998. Their daughter, Jimin Kim, was born on April 18, 2000 and their son, Hyoungmin Kim, was born on Feburary 17, 2004.

THESIS ABSTRACT

AN EVALUATION SYSTEM FOR MECHANICAL AND ELECTRICAL CHARACTERIZATION OF MEMS DEVICES

Seong Jin Kim

Master of Science, May 9, 2009
(B.S. Electronic Engineering, Yonsei University, Seoul, South Korea, 1992)

95 Typed Pages

Directed by Robert N. Dean

The evaluation of MEMS devices during the developmental phase prior to packaging is challenging. However, evaluating a MEMS device in die form can be useful, as its electrical and mechanical test results can provide useful feedback to improve the design, modeling and fabrication process. It can be worthwhile to evaluate the performance of MEMS devices in regard to various parameters, such as in various gas chemistries and at different pressures, and with and without mechanical and/or electrical excitation. From these tests, the design and manufacturing processes can be adjusted before packaged devices are available for in-depth testing.

To accomplish this goal, a vacuum chamber based MEMS evaluation system has been developed for electrically and mechanically evaluating MEMS die. The system consists of a bell jar vacuum system with a pressure range from 0.050 Torr to ambient pressure. Additionally, the vacuum system has been constructed to allow other gases to be injected into the vacuum chamber for device testing. A machined plastic fixture is used to mount the bare die during testing. It attaches to a small electromechanical shaker that resides inside the vacuum chamber for dynamic mechanical testing of the MEMS device. Two laser interferometers are used through the glass bell jar to then

measure the relative motion of two locations on the die, thus allowing the transmissibility and the range of a microstructure's motion to be measured. The evaluation system also has nine electrical feedthroughs for external connection to the MEMS die or to other test equipment located inside the chamber. Additionally, a graphite heating stage has been integrated into the chamber for thermal testing.

To demonstrate the usefulness of this evaluation system, electrical and mechanical tests have been performed on several MEMS devices and systems to measure the mechanical frequency response, the mechanical quality factor in various gases at different pressures, and the closed loop operation with integrated electronics. This system is directly compatible with the microfabrication clean room. Thus, it allows early testing of new devices before packaging has been completed.

ACKNOWLEDGMENTS

My foremost thanks goes to my advisor, Assistant Professor Robert Dean, who has guided and encouraged me academically and financially. I could not have imagined having a better advisor for my study. Without his knowledge, wisdom, and having given me the opportunity to work with him, none of this work would have been possible.

I also would like to thank Professor Flowers for his help and support for my research. His constructive feedback and support at critical stages have been immensely helpful in completing this endeavor. I sincerely thank Professor Wilamowski and Professor Roppel for serving on my committee. Their insight into my research of the analysis and testing of MEMS devices has been invaluable.

Additional thanks goes to Mr. Palmer for his assistance with the construction of the MEMS evaluation system.

One of the most precious persons who has been with me in every moment is my wife Eun Jung An. I would like to thank her not only for the many sacrifices she has made to support and understand me in undertaking my study, but also for guiding me along the right path all my life. I would like to thank my children Jimin and Hyoungmin for their ceaseless love and smiles which have strengthened me. I would also like to give big thanks to my parents, Si-Hwan Kim and Byoung-Won Suh, for praying for and always being there for me.

Finally, and most vitally, I would like to thank so much the almighty God, not only for giving me a faith, a wisdom and health to complete a graduate study, but also for guiding me along the right path all my life.

Style manual or journal used Journal of Approximation Theory (together with the style known as “aums”). Bibliograpy follows van Leunen’s *A Handbook for Scholars*.

Computer software used The document preparation package TEX (specifically LATEX) together with the departmental style-file `aums.sty`.

TABLE OF CONTENTS

LIST OF FIGURES

LIST OF TABLES

CHAPTER 1

INTRODUCTION

In contrast to the very standardized design process for VLSI, MEMS device design requires the consideration of not only electrical and mechanical functionality, but also the complex fabrication process and its influence on the design, if the MEMS device is fabricated using conventional IC fabrication techniques. Additionally, a time consuming iterative process covering the entire device realization process, from design through packaging and test, may be required for successful device development. In spite of an iterative design process, such as analysis and simulation with a Computer-Aided Design (CAD) tool [1], testing the packaged MEMS device without fully evaluating the device at die level may result in the discovery of unexpected device characteristics, which could result in a whole new iteration.

Various on-wafer testing systems aid in finding an optimal process with minimized production costs through identifying possible errors and by maximizing yield. Similarly, a general purpose MEMS evaluation system, that can be used prior to device packaging, can be useful in minimizing the iterative MEMS development process. Once the device is fabricated according to the initial design, it can then be tested and characterized by the MEMS evaluation system.

The MEMS evaluation system in this research endeavor was constructed with off-the-shelf components, consisting of a vacuum bell-jar chamber with substrate quartz lamp heaters and a heater controller, a small electromechanical shaker, two laser displacement interferometers and their controllers, a pressure transducer, a digital pressure meter, and a signal analyzer, a vacuum pumping system, and various vacuum system fittings and plumbing. The vacuum system supported a pressure inside the bell-jar between 0.05 Torr and ambient pressure. The internal graphite heater could heat the attached device and its surroundings to 200°C. The chamber possessed a gas inlet for the supply of various gases. The glass bell-jar could be used with two laser interferometers to measure useful mechanical properties of the MEMS device, such as the range of motion, the natural frequency, the transmissibility and the quality factor. The small shaker provided the MEMS device with a mechanical stimulus in a frequency range of 400Hz to 3.6 kHz. Additionally, the evaluation system had nine electrical feedthroughs that provided the MEMS device and the small shaker with electrical connections. The pressure transducer and digital readout meter had a resolution of 0.001 Torr. The dynamic signal analyzer had two input channels used to receive the two interferometer outputs, and one source output to control the small shaker. The evaluation system utilized the Microfabrication Laboratory mechanical vacuum pump, which was connected to the outlet port of the vacuum chamber using flexible plastic pipe.

A literature review of relevant background information is presented in Chapter 2. This includes MEMS features, analysis tools in design, and measurement methods.

System requirements for evaluating MEMS devices, consisting of stimulus and measurement, are presented in Chapter 3. A discussion on currently available commercial MEMS evaluation systems is also presented.

A detailed discussion on the MEMS evaluation system developed through this endeavor is presented in Chapter 4. It describes mechanical, environmental, electrical, and optoelectrical requirements of the system for various MEMS device evaluation procedures, design philosophy, and how the system is constructed. Lastly, the capability of the system is presented.

The results from the evaluation of various MEMS devices and systems, performed with this evaluation system, is presented in Chapter 5. This includes closed-loop damping control at low pressure, relative velocity sensor performance at low pressure, capacitance vs. pressure and transmissibility vs. pressure in various gas environments.

CHAPTER 2

LITERATURE RIVIEW

2.1 MEMS Features

Microfabricated mechanical elements, structures, electrodes, traces, capacitors, piezoresistors and sometimes even semiconductor devices, are integrated to realize complex Microelectromechanical Systems (MEMS) devices such as sensors [2], actuators [3], RF switches [4] and energy conversion devices [5]. Such diverse functionality in MEMS devices has required a new approach to modeling and testing to ensure proper functioning of the system. MEMS devices are often fabricated with processes borrowed for integrated circuit (IC) manufacturing techniques. The two primary manufacturing techniques for Si based MEMS devices are Bulk micromachining [6] and Surface micromachining [7]. These micro-fabrication processes have some limitations, which can result in defects such as broken structures, under/over etching and stiction. Moreover, due to the miniature size of the MEMS devices, mechanical characteristics are sensitive to variation in material properties and to microfabrication limitations and tolerances. Therefore, evaluation and recognition of mechanical behaviors as well as electrical performance are important in MEMS device development.

2.2 Analysis Tools for MEMS

MEMS analysis tools allow for predicting the MEMS device's behavior and optimizing the various design parameters prior to device fabrication. While the analysis tools for electronics are well established, the tools for MEMS devices are not yet well established due to the relative youth of MEMS technology and the complexity involved.

The design flow in the MEMS CAD design environment includes iterative mechanical schematic generation and MEMS simulation in the early design stage. Most analyses and simulations possess two levels, as shown in Figure 2.1: the physics level for the detailed behavior in 3-D and the system level for the behavior of the entire system. Tools for the physics level typically use finite element (FE), finite volume (FV), or boundary element techniques.[8-9]

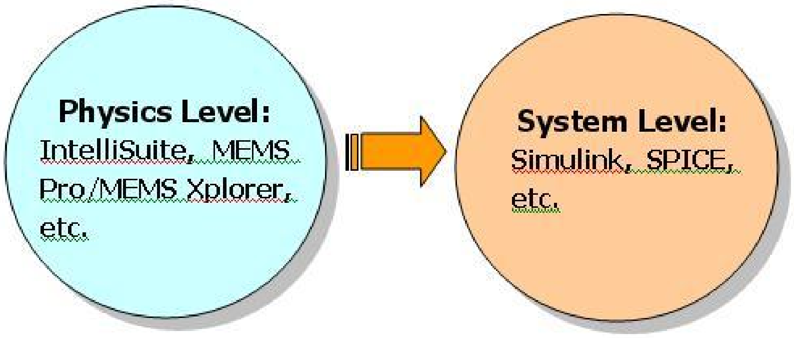

Figure 2.1: Two Simulation Levels

2.2.1 Finite Element Analysis (FEA)

FEA divides the device into very tiny elements through a meshing process, which is the first activity at the physics level. This enables the analysis of complex geometries of MEMS devices in points of mechanical and thermal interest. Examples of commonly used FEA tools include CoventorWare [10], IntelliSuite [11], and MEMS Pro/MEMS Xplorer [12].

2.2.2 System Level Analysis

In the system level analysis, the performance of a MEMS device, which was modeled with a lumped element model, can be evaluated using tools such as Simulink or SPICE, where the MEMS device is described by ordinary differential equations and nonlinear functions. An accelerometer, for example, can be modeled using a proof mass, a spring, and a damper. An example of the system level analysis for a commercial accelerometer, the Analog Devices ADXL180, is shown in Figure 2.2.

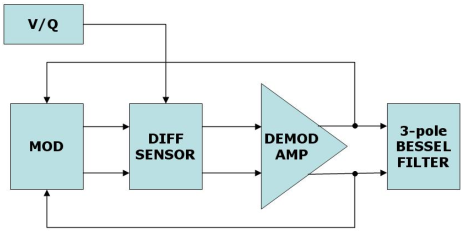

Figure 2.2: System Level Model of the ADXL180 MEMS Accelerometer [50]

•Simulink: Simulink enables the implementation of a nodal model [13] for investigating the dynamics of a MEMS device. Simulated result data can easily be post processed using Matlab [14].

•SPICE: SPICE is one of the ordinary differential equation (ODE) solvers that is used at the system level. Although initially developed for simulating electrical circuits, it is a powerful tool that can be used to model any linear system. A PC version, PSPICE [15], is commonly used.

2.2.3 Contamination Analysis

Contamination analysis is a process to analyze and predict feasible damages of physical geometries of a microstructure occuring during a fabrication process, which affect the structure or material properties. The contamination leads to faulty MEMS behavior. Therefore, predicting the effect of the contamination in the design stage is important to improve the quality of MEMS products. On another hand, contamination analysis [16] using software simulation tools can also be a useful MEMS evaluation method. As the first step, Contamination-Defect-Fault (CODEF) simulation tools perform simulations using microfabrication process recipe data, contamination properties, and microstructure layout, which generates fault macro models of the various defective microstructures. For example, a CODEF simulation for a microsensor might reveal defects such as shuttle defect, comb defect, and flexure defect. The photo of a comb defect is shown in the Figure 2.3. Based on the locations and feasible defects from CODEF, a mechanical simulation with ABAQUS can be performed to acquire some defects which can cause complete failure in the device. So, simulating the MEMS device in the design phase can be considered to be an efficient means for MEMS device development.

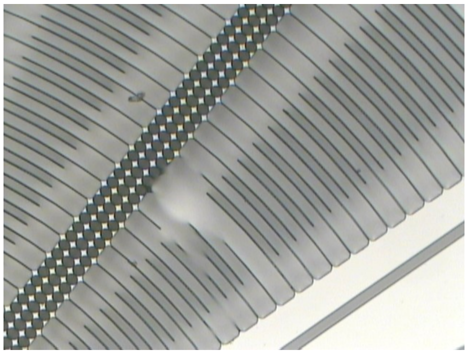

Figure 2.3: Photograph of Comb Defect

2.3 Measurement Methods

Many useful test, evaluation, or monitoring methods have been proposed to verify that the MEMS device mechanical characteristics and motion match the design requirements. There are two basic categories of testing methods for measuring MEMS mechanical characteristics [16]. One is a contact method using a microprobe or mass loading to measure a deflection, which is a kind of static test for measuring mechanical properties of a MEMS structure or material. The other is a non-contact method which includes electrical or optical technology. Examples include microtension test, microbeam bend test, axisymmetric plate bend test, resonant frequency test, and M-test to measure Young's modulus or the fracture strength [17]. Those methods need excitation of the MEMS structure to measure the changes either electrically or optically.

2.3.1 Electrical Method

This method makes use of a piezoresistive, a piezoelectric or a capacitive property.

- Piezoresistivity: This property is a material effect where the material experiences a change in resistance due to an applied strain. Semiconductor materials experience the piezoresistive effect while metal films and foils experience a change in resistance in response to an applied strain due to the geometric effect. Therefore, a metal foil strain gauge uses the geometric effect and not the piezoresistive effect.

- Piezoelectricity: Certain classes of crystals produce an electric charge when they experience a strain, and they also deform in response to an applied electric field. Quartz, zinc oxide, and lithium niobate are examples of piezoelectric materials.

- Capacitive Technique: For example, one fixed electrode and one or more movable electrodes, or two fixed electrodes with a movable dielectric material, experience a change in capacitance in response to a change in the electrode configuration or the dielectric material.

2.3.2 Optical Method

Optical sensing methods primarily utilize the modulating properties of an optical frequency electromagnetic wave. The non-contact sensing nature of these methods is suitable for measuring the MEMS mechanical characteristics without a mass loading effect.

- Laser Doppler Velocimetry: The laser light reflected from the moving MEMS surface will have a shift in frequency by an amount proportional to the velocity of the surface compared to that of the radiated laser light source. The optical setup of laser Doppler velocimetry is presented in Figure 2.4.

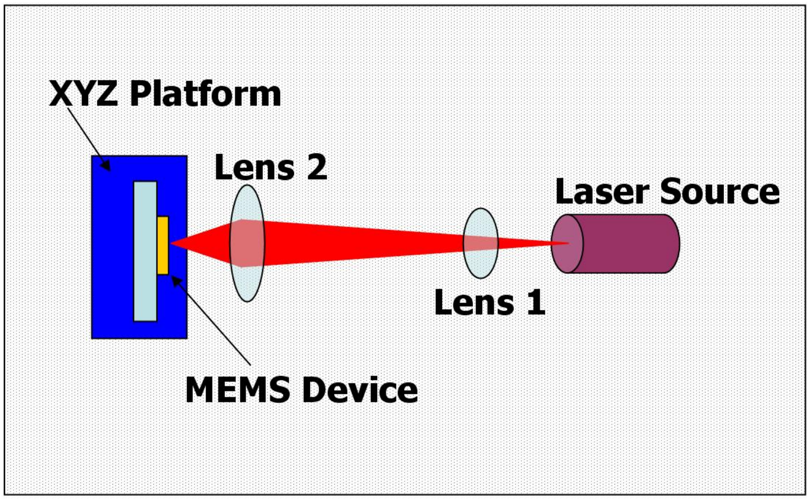

Figure 2.4: Laser Doppler Velocimetry Setup [16]

- Interferometry: The principle of interferometry is that two coherent optical beams will form a interference or fringing pattern that is dependent on the phase difference between the two beams. Typically, a single incident source beam of light is split into two identical beams, using a beam splitter and mirror, and travel along two paths of either continuous or stroboscopic illumination.

The illustration of Figure 2.5 presents the principles of interferometry. The He-Ne laser beam is split by a first beam splitter (BS1) into a reference beam and a measurement beam. After passing through a second beam splitter (BS2), the measurement beam is focused onto the object under investigation and then reflected from the object. This reflected beam is deflected by the second beam splitter (BS2), then merged with the reference beam by a third beam splitter (BS3). Finally, they reach the detector. As the length of the reference beam is constant over time, a movement of the object under investigation generates a fringe pattern on the detector. One complete dark-bright cycle on the detector corresponds to an object displacement of exactly half of the wavelength of the laser

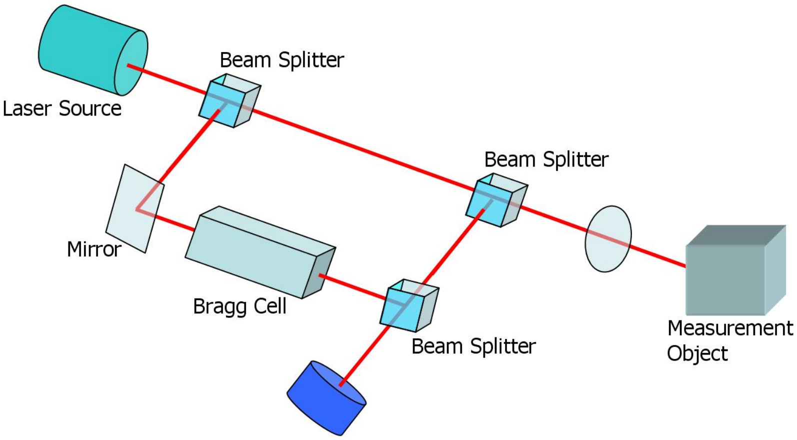

Figure 2.5: Illustration of Interferometry [18]

used. As an example, an illustration of a stroboscopic interferometer system is presented in Figure 2.6. Electronic Speckle Pattern Interferometry (ESPI) is also used for measuring the vibration of

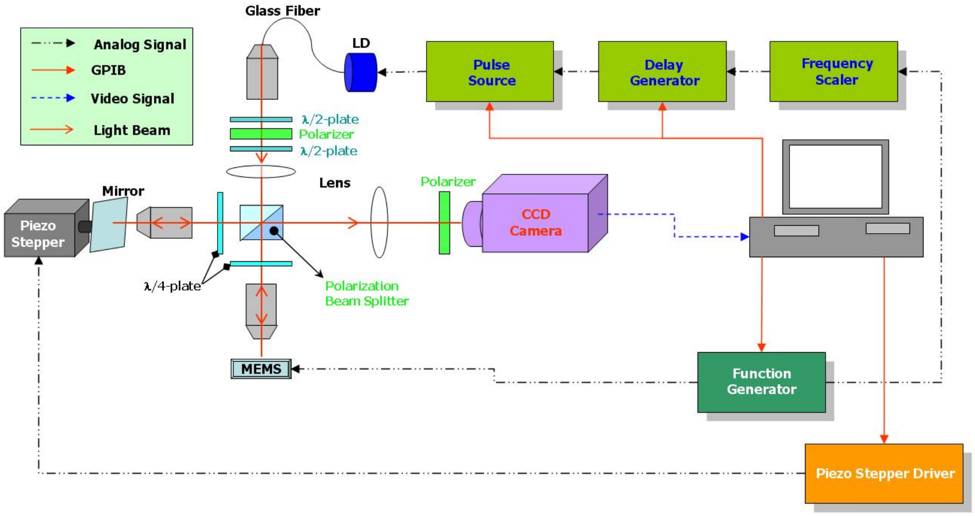

Figure 2.6: Stroboscopic Interferometer System [19]

microstructures possessing a rough surface [20].

• Optical Microscope: This method is a non-interferometry method. The Computer Microvision System (CMS) developed by MIT is composed of a light microscope with a movable stage, a

CCD camera, a signal generator, and a PC [21]. A MEMS device placed on the stage is exposed to a periodic LED light source and imaged by the microscope with a CCD camera. The LED is strobed once per stimulus period at a chosen phase to produce a snapshot of the device position. The repeated snapshots at several stimulus phases and at several locations are processed and result in the capturing of the motion of the device through one period. An illustration of the Computer Microvision System is presented in the Figure 2.7.

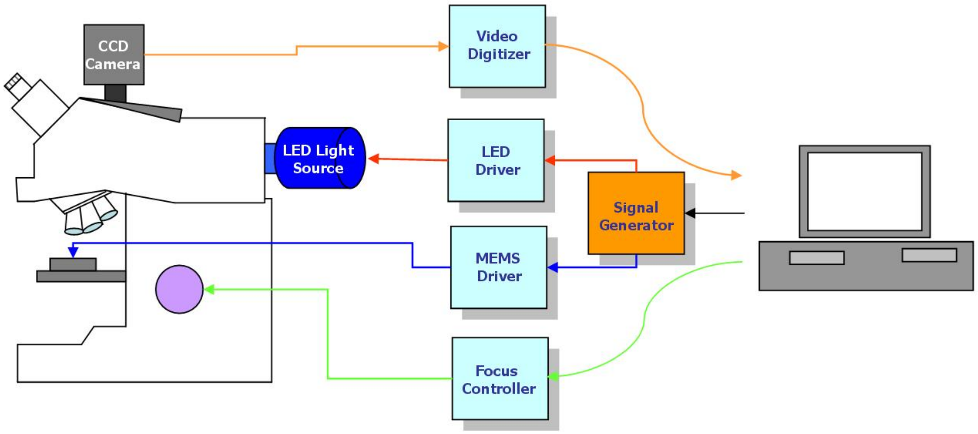

Figure 2.7: Computer Microvision System [22]

- High Speed Cine Photomicrography [23]: This method was developed for capturing the image of fast moving structures due to optical magnification by combining a ultra high speed camera and a microscope. This method captures the position of moving parts in microdevices with respect to time. To analyze extremely fast movements of microdevices , a pulsed light source with high constant intensity is needed. Therefore, the visualization of the movement of the microdevices is performed using the stroboscopic principle. During the measurement, picture taking is repeated several times and then visualized at subsequent points of time, which results in a sequence of images.

CHAPTER 3

TESTING OF MEMS DEVICES

3.1 System Requirements

In conventional IC testing, wafer level testing is typically performed using precisely controlled wafer probes. Figure 3.1 presents an illustration of the the input, output, and environments for conventional IC testing. In MEMS devices, excitation as an input is used under a wider range of environmental conditions. The output of the MEMS devices can be an optical signal or an electrical signal, as presented in Figure 3.2. The requirements to accomplish the various types of MEMS

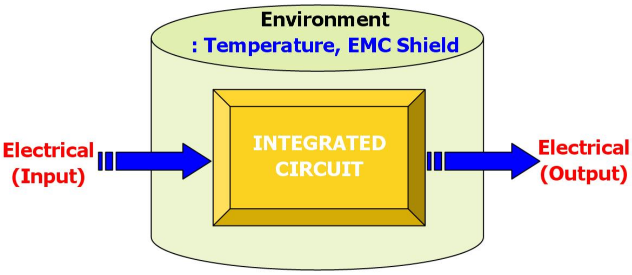

Figure 3.1: System Requirements for Testing Integrated Circuits

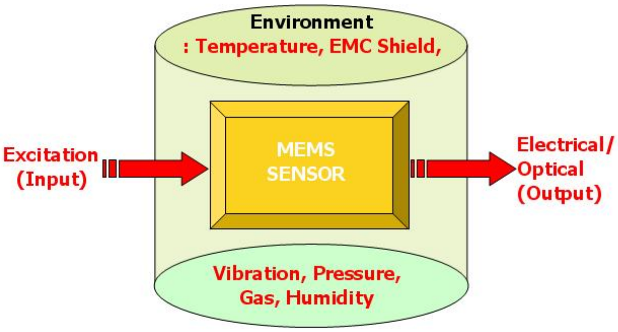

Figure 3.2: System Requirements for Testing MEMS Device

testing can be very sophisticated. The MEMS evaluation system needs to be equipped with the capabilities for analyzing the mechanical and electrical characteristics of the device. These testing capabilities heavily depend on the type of MEMS Device Under Test (MDUT). The system must provide electrical and mechanical stimuli to the MDUT and then detect the corresponding response of the device. Electrical and mechanical stimuli are usually device specific. Therefore the stimuli must be tunable with adjustable parameters, such as amplitude, frequency, bandwidth, duration, etc. Additionally, the evaluation system should have the capability of evaluating environmental effects, such as ambient gas pressure and temperature.

In order to evaluate some MEMS devices such as accelerometers, gyroscopes, pressure sensors, and infrared (IR) detectors, the evaluation system is designed for operation in a low pressure or a specific gas environment. This type of evaluation system can be called a “closed platform”. A photograph of the SUSS PAP200, manufactured by SUSS MicroTech, is presented in Figure 3.3. This closed platform evaluation system is used not only for testing pressure sensors from 100mbar up to 50bar absolute pressure, but also for probing in a controlled gas atmosphere and/or with controlled

Figure 3.3: Closed Platform Test Equipment: SUSS PAP200 [24]

humidity. The chamber has a top-side view-port for the microscope as well as four additional view-ports. On the rear side, 192 high pressure electrical feedthroughs are located for the chuck stage for probe-heads, probe-card, and chamber temperature measurement. Five fluidic feedthroughs can be used with several connectors to the pressure supply system to supply atmospheric pressure. The pressure supply system of the evaluation system consists of a compressor, a booster, a vacuum pump, and a controller. The compressor generates a pressure of up to 30 bar, and the booster expands the compressor's working pressure to 80 bar. The microscope mounted on the top window provides features such as recording images and pattern recognition.

An "open platform" evaluation system can evaluate differential and absolute pressure sensors, microphones, and micromirrors in an ambient environment. A photograph of the Model 622-A, manufactured by EM Optomechanical, is presented in Figure 3.4 as an example of the open plat-

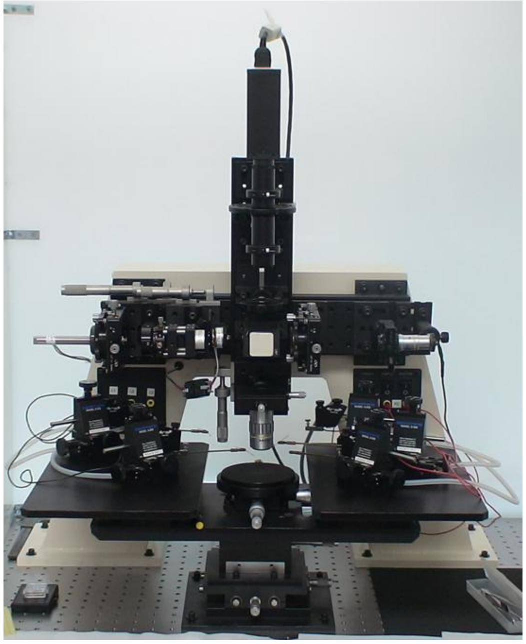

Figure 3.4: Open Platform Test Equipment: EM Optomechanical 622-A (courtesy Auburn University)

form. This 3D MEMS profiler is composed of a vibration isolation platform, two left-hand vacuum base probe micropositioners, two right-hand vacuum base probe micropositioners, a non-coherent green LED as a standard light source, a 2/3-inch black & white CCD camera, and an image processing system.

The image processing system consists of a National Instruments analog output board, a Data Acquisition (DAQ) PCI board, and device drivers. An application software package, MEMScript^{TM}, provides analysis features and the ability to control MEMS devices and to make real time measurements of performance, such as pattern matching, phase shifting interferometry, decision making capability, stroboscopic imaging, and arbitrary waveform output. The photographs in Figure 3.5 presents a picture of MEMS device on the vibration platform and application software of MEMScript^{TM}.

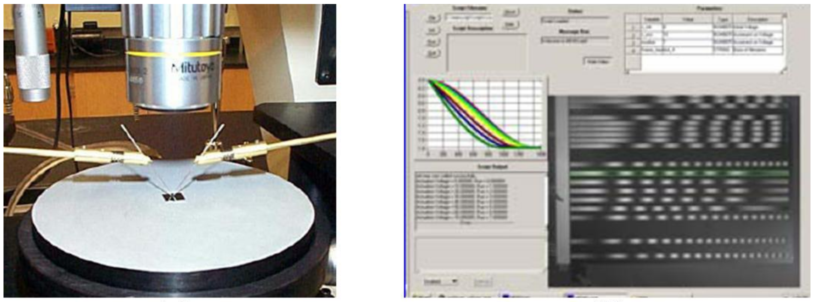
(a) (b)

Figure 3.5: EM Optomechanical 622-A: (a) MEMS device on the Vibration Platform, (b) GUI Screen of MEMScript^{TM} [25]

3.1.1 Electrical Stimulus

There are several excitation method for MEMS devices, such as, electrostatic stimulus, acoustic stimulus, electrothermal stimulis, etc. [20, 26]. For a MEMS device that responds to an electrical stimulus, the stimuli is an applied voltage or current. If a Built-In Self-Test (BIST) function is implemented in the electronics of the MEMS device, the required physical stimulus can be applied to the device by applying an electrical signal to the BIST input pin, without externally applying an excitation force [27-28]. As an example of a MEMS device with a BIST function, the Analog Devices' ADXRS300 angular rate sensor includes a BIST feature that allows two external signals to be applied to the device to cause the internal microstructure to experience the same response as it would to angular rates of $+55°$/s and $-55°$/s, respectively. This BIST scheme is designed so that a microcontoller supplies the self-test signals to two BIST pins and then checks the rate from the rate pin. However, MEMS devices at die level usually need external excitation to be tested.

- Electrostatic stimulus: The electrostatic stimulus uses the principle that an attractive force will be produced between two parallel electrodes (or plates) when a voltage is applied between them. An illustration of an electrostatic parallel plate actuator (PPA) is presented in Figure 3.6. The energy stored in PPA without fringing effect, which is expressed as [29]:

$$W = \frac{CV^2}{2} = \frac{\varepsilon_o \varepsilon_r A V^2}{2L}, \tag{3.1}$$

may be differentiated with respect to L in order to obtain the force between the two plates. This results in the following nonlinear relationship [29] between force and voltage:

$$F = \frac{dW}{dL} = \frac{\varepsilon_o \varepsilon_r A V^2}{2L^2}. \tag{3.2}$$

However, this method often requires high voltages in order to achieve sufficiently high electrostatic forces, which often results in utilizing narrow gap microstructures fabricated using surface micromachining process. Comb-drive actuators, gap closing actuators and scratch drive actuators are other types of electrostatic actuators.

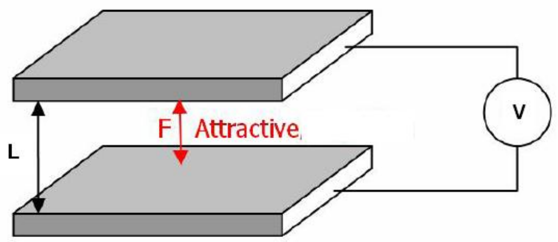

Figure 3.6: Electrostatic Parallel Plate Actuator

- Electrothermal Stimulus: The principle of the electrothermal stimulus is that two materials possessing different Coefficients of Thermal Expansion (CTE) are bonded together to realize a composite structure that bends in response to a temperature change above or below the temperature at which materials were bonded together. An example device is a thermal vertical bimorph actuator [30-31]. Joule heating can be used as the electrothermal stimulus by passing an electrical current through an resistive heater integrated into the MEMS device [26].

- Piezoelectric Stimulus: An applied voltage across the electrodes of a piezoelectric material, whose crystal structure is asymmetric, produces a deflection. The most commonly used piezoelectric material is lead zirconate titanate (PZT) [32].

- Electromagnetic stimulus [33]: An electromagnetic force (Lorentz force) occurs in a direction perpendicular to the current and a magnetic field when a current flows within a conductor in the magnetic field. The externally applied magnetic field may be produced by a permanent magnet of by an electromagnet, which is brought into close proximity to the MEMS device.

3.1.2 Non-electrical Stimulus

- Vibration: The vibration stimulus provides sinusoidal or wide bandwidth vibrational motion or velocity to the MEMS device. An electromechanical shaker is often used to produce a vibration stimulus. Accelerometers [34] and velocity sensors [35] are examples of MEMS devices that may be evaluated using a vibration stimulus. A photograph of the V830 Electrodynamic Shaker manufactured by LDS is presented in Figure 3.7.

Figure 3.7: LDS V830 Electrodynamic Shaker [36]

• Rotation: Some MEMS devices, such as MEMS gyroscopes, directly respond to angular rate, where the applied angular rate may be constant or time varying. Additionally, the centrifugal force, resulting from an object, which is located a fixed distance from the center of rotation, can be used as an acceleration stimulus for a MEMS accelerometer. A photograph of a high speed angular rate table is presented in Figure 3.8.

• Pressure: Applied ambient gas pressure can be a stimulus to MEMS devices designed to respond to pressure changes, such as MEMS pressure sensors [37]. It can also be a stimulus to other MEMS devices that are affected by ambient gas pressure, such as resonating structures [38], where the pressure stimulus here would change very slowly over time.

• Acoustic: Sound is actually high frequency pressure waves that propagate in the ambient fluid that surrounds the MDUT. Although MEMS microphones are designed to respond to sound,

Figure 3.8: MEMSense High Speed Angular Rate Table (courtesy Auburn University)

some MEMS devices, such a gyros, may adversely respond to sound [39]. An acoustic chamber may be used in evaluating MEMS devices with this stimulus.

• Electromagnetic Radiation: This stimulus could include RF energy, IR, visible light, UV, and X-rays. Different types of evaluation equipment are required for each of these types of radiation. Many MEMS devices could benefit from evaluation with radiation stimuli, including RF devices, thermal sensors, optical devices, and radiation sensors.

3.1.3 Measurement

Sensing the mechanical movement of a MEMS device requires the appropriate measurement methods. As discussed in Chapter 2.3, electrical measurement method includes piezoresistive, piezoelectric and capacitive techniques. These measurement methods can be implemented in a MEMS device to convert mechanical movement into an electrical signal. When using the optical measurement methods, a light beam interacts with one or more movable microstructures on the

MEMS device. As a result, microstructure motion can then be measured by detecting changes in intensity, phase, wavelength, frequency, and/or spatial position. The optical measurement method has a merit of being a non-contact technique, which usually does not affect the microstructure motion during device testing.

3.1.4 Fixturing

Some type of fixture is usually required to hold or mount the MEMS device during evaluation. This can be particularly challenging for bare die MEMS devices, as they can be very fragile. Fixturing is very much application specific.

3.2 Commercial MEMS Evaluation Systems

3.2.1 Open System

- Laser Doppler Velocimetry: The Polytec's LSV 6000, a laser surface velocimeter, is an example commercial system that uses the laser Doppler velocimetry technique. This system consists of a sensor head and a controller. The sensor head is a light source using a visible diode laser, and the controller is a signal processor that evaluates the Doppler frequency change of the laser signal by means of FFT analysis. A photograph of a LSV 6000 is presented in Figure 3.9.

Figure 3.9: Laser Doppler Velocimeter: Polytec LSV 6000 [40]

- Interferometry:

▷ Micro System Analyzer: The Polytec MSA-500 uses a white light interferometry method for high resolution topography measurement. This system can visualize and measure system in-plane and out-of-plane resonances and transient responses of microstructures of MEMS devices. A photograph of a MSA-500 analyzer is presented in Figure 3.10.

Figure 3.10: Interferometer: Polytec MSA-500 [41]

▷ Dynamic MEMS Measurement System: The Wyko NT1100 system with the DMEMS option is a dynamic and static MEMS metrology system that uses phase-shifting and white light vertical scanning interferometry. The capabilities for this system include a 3D visualization of moving MEMS devices as well as the measurement of in-plane and out-of plane dimensions. A photograph of a Wyko NT1100 manufactured by Veeco is presented in Figure 3.11.

3.2.2 Closed System

- Pressure Sensor Tester (SUSS PAP200): This system is a probe station primarily designed for evaluating pressure sensors from 100 mbar up to 50 bar absolute pressure. Additionally, this system

Figure 3.11: Dydnamic MEMS Measurement System: Wyko NT1100 [42]

can simulate a controlled gas atmosphere with controlled humidity. As shown in Figure 3.12, the pressure chamber has a top-side view-port for a microscope and four additional view-ports. On the rear side, 192 multi-pole electrical feedthroughs are located for the chuck stage, measurement cables, chamber temperature measurement, and operating a temperature controlled chuck. Five fluidic feedthroughs for a relative pressure sensor are connected to the pressure supply system.

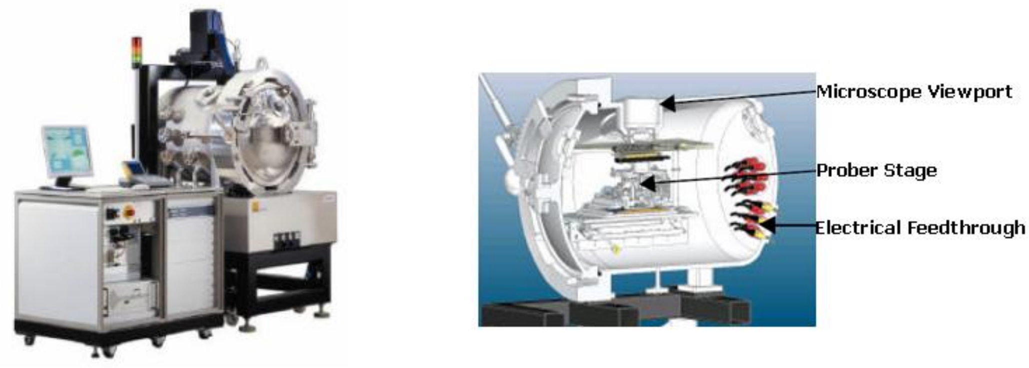

Figure 3.12: Pressure Sensor Tester: SUSS PAP200 [43]

• Micro System Analyzer (Polytec MSA-400) combined with a vacuum chamber: This system is a combination of a vacuum chamber and a micro-scanning laser Doppler vibrometer for characterizing MEMS devices over a wide range of ambient pressures. Through a window in the vacuum chamber, the micro system analyzer measures the motion of a MEMS device excited by broadband stimuli, including periodic chirp and white noise. A photograph of a MSA-400 is presented in Figure 3.13.

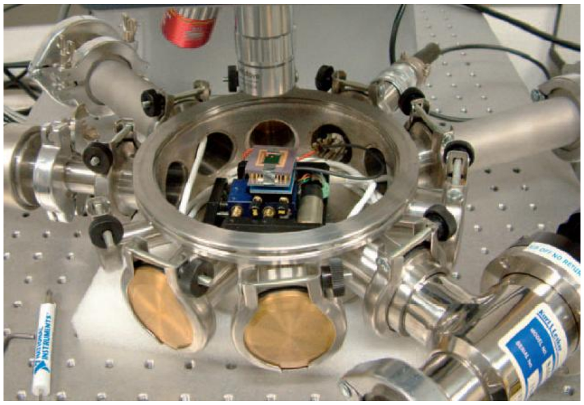

Figure 3.13: Micro System Analyzer with Vacuum Chamber: Polytec MSA-400 [44]

CHAPTER 4

MEMS EVALUATION SYSTEM

4.1 System Requirements

The requirements for the MEMS evaluation system to test MEMS devices can be categorized into four factors: stimulus, environmental, electrical, and measurement requirements. Due to the mechanical and electrical functionalities of the MEMS device, the equipment for the stimulus and measurement can be varied according to the device application. The closed system can simulate various packaging environments and should be equipped with an electrical interface to provide the needed electrical signals and to receive output signals.

4.1.1 Stimulus Requirement

The system is equipped with an electromechanical shaker that can shake the MDUT in a controlled fashion for the measurement of mechanical characteristics such as mechanical transmissibility and quality factor. As the system is designed for various tests using the MEMS velocity sensor, other stimulus equipment, such as a rate table, a microphone, or an electromagnetic radiation source, are not needed.

4.1.2 Environmental Requirement

To simulate various packaging conditions at pressures lower than ambient, the pressure needs to be controlled, and various gases may need to be injected. When the system is a closed platform and optical measurement equipment is used, the chamber should have a transparent window for the light source of the optical equipment to shine onto the device surface.

4.1.3 Electrical Requirement

The system should provide an electrical interface, such as an electrical feedthrough, which can be connected between the external equipment and the MDUT in the chamber. The electrical feedthrough should also have enough pins for electrical power, control and measurement signals.

4.1.4 Measurement Requirement

Since many unpackaged MEMS devices lack on-chip electronics for converting the applied mechanical stimulus to an output electrical signal, external optical detection equipment, such as a laser velocimeter, a laser interferometer, or an optical microscope, may be used. However, if the MDUT possesses suitable on-chip electronics, then electrical characteristics can be measured using an oscilloscope, a LCR meter, or a multi-meter.

4.2 Design

The system configuration schematic of the MEMS evaluation system is presented in Figure 4.1. The system was designed as a closed platform type. The bell jar vacuum chamber has a small shaker, which is located on the heater plate. Since the MDUT is mounted on a small shaker located on the graphite heat plate, the MDUT cannot be heated by the heater. Therefore, the heater and the small shaker are not used at the same time. If the heater is to be used, then the shaker is removed from the bell jar first, and the MDUT is then placed on the plate. A MEMS device is attached to the small shaker. Outside the bell-jar, two optical laser interferometers and their controllers are connected to the signal analyzer, which also controls the small shaker in specific frequency and displacement ranges. A pressure transducer is attached to a mechanical feedthrough, and a readout meter displays the chamber pressure. The vacuum pump and gas cylinder are connected to the bell

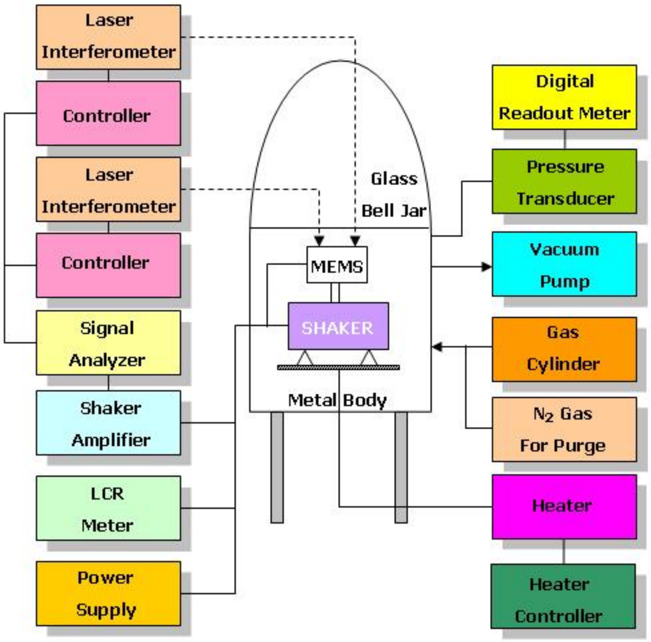

Figure 4.1: System Configuration Schematic

jar through the gas lines. With this configuration, the evaluation system can excite MEMS devices and measure the electrical and mechanical characteristics of them.

4.3 Construction

As presented in the Figure 4.2, the constructed MEMS evaluation system is assembled using a glass bell jar with a L-gasket, a metal base with electrical feedthroughs and a heater, an analog pressure gauge, and a mechanical vacuum pump.

- Bell-jar Chamber: A glass bell-jar chamber was chosen for the vacuum chamber. The glass bell-jar size is 12” in height with a 12.5” diameter. The chamber has a transparent glass bell-jar which is suitable for laser interferometer usage. The chamber is mounted on the four stiff metal legs. In the middle of the glass bell-jar and metal legs, five feedthroughs for an electrical connector,

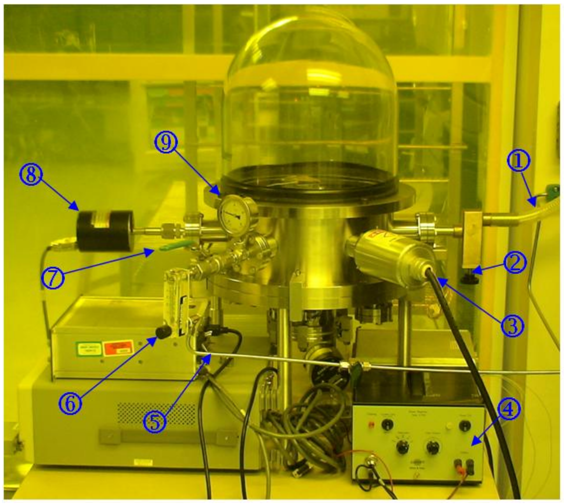

①: Vacuum Outlet Line to Pump
②: Manual Bellows Valve for Vacuum
③: Heater
④: Power Amplifier Type 2706
⑤: Gas Inlet Line from Cylinder
⑥: Precise Control Valve in Flow Meter
⑦: Main Ball Valve for Injecting Gas
⑧: Pressure Transducer
⑨: Analog Pressure Gauge

Figure 4.2: MEMS Evaluation System: Front View

a heater, a pressure transducer, several valves, and an analog pressure gauge are located around the metal chamber body, as presented in Figure 4.2 and Figure 4.3. On the bottom of the metal body,

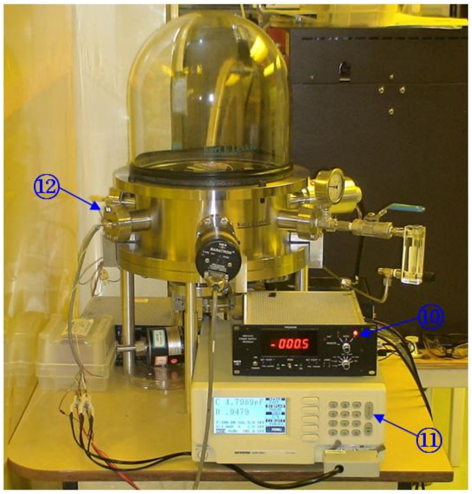

⑩: Digital Readout for Pressure Transducer
⑪: LCR meter
⑫: Electrical Feedthrough with 9 D-sub Connector

Figure 4.3: MEMS Evaluation System: Side View

three additional feedthroughs are also located that can be used for expansion. An inlet gas line is connected through a ball valve and a precise control valve with a flow meter for fine control of the gas supply, and an outlet gas line through a manual bellows valve to the vacuum pump. An electrical feedthrough with a 9-pin D-sub connector is also located in the chamber body and can provide nine electrical interfaces, as presented in the Figure 4.3.

• Stimulus Equipment: A photograph of an Mini-shaker Type 4810, manufactured by B&K, is presented in Figure 4.4, which is located on the heater plate inside the chamber. The small shaker is connected to a power amplifier driven by the dynamic signal analyzer. The power amplifier provides the small shaker with regulated power to vibrate at a specific amplitude and/or over a bandwidth of frequencies. A photograph of the Power Amplifier Type 2706, manufactured by B&K, is presented in Figure 4.2. For securely mounting the MDUT, a 10*32NF threaded hole is located at the center of the shaker head. Therefore, it is relatively easy to attach a printed circuit board (PCB) to the shaker hole.

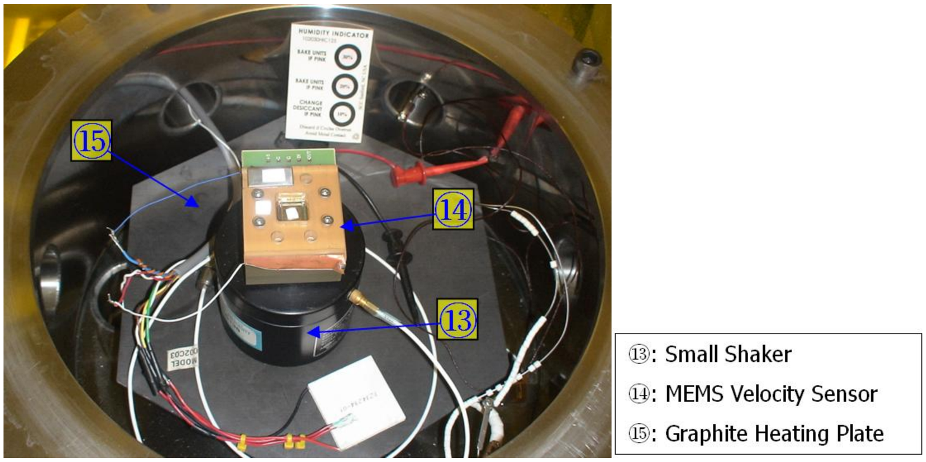

Figure 4.4: MEMS Evaluation System: Inside View

• Vacuum Pumping System: A mechanical vacuum pump is connected to the outlet port of the vacuum chamber using flexible plastic pipe. As the pumping system is the combination of the vacuum pump, the chamber, and its sealing, the vacuum system components also depend on how well the bell-jar chamber is sealed. There may be many leaking places at junctions between feedthroughs and the chamber. Leaks can occur at many locations in the vacuum system. A photograph of the Model 5KC36PN4 vacuum pump, manufactured by General Electric, is presented in Figure 4.5.

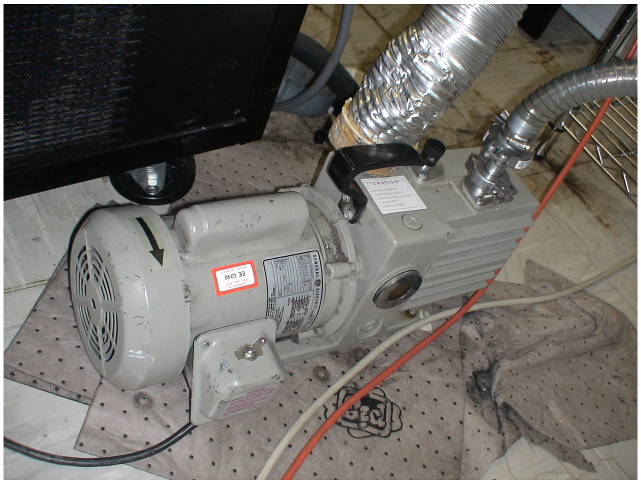

Figure 4.5: Photograph of the Mechanical Pump

- Optical Measurement System: A laser vibrometric system is composed of a laser unit and a vibrometer controller. A photograph of the optical measurement system including the signal analyzer is presented in Figure 4.6. The constructed system has two laser units; the motion of the moving part of a MEMS device is measured by the first laser interferometric system, and the second interferometric system is used to measure the motion of the frame of the MEMS device. The two output signals are recorded simultaneously, then the transmissibility of the MEMS device can be determined using the dynamic signal analyzer. The dynamic signal analyzer is an instrument that processes input signals to yield various information about the signals as opposed to an oscilloscope, which simply displays the input signals. The analyzer has an FFT mode for calculating the frequency spectrum of a time domain signal.

- Electrical Measurement System: The electrical measurement system of the evaluation system consists of a LCR meter, a digital oscilloscope, and a digital multimeter (DMM). They are

Figure 4.6: Photograph of the Optical Measurement System (two laser units, two controllers, and a signal analyzer)

located outside the vacuum chamber and are connected to the wires coming out from the electrical feedthrough of the chamber. A tripple output power supply is often a necessary piece of equipment to supply power to the MDUT.

• Gas Supply: A gas is injected from the gas cylinder outside the chamber and controlled by a ball valve and a precise control valve of the vacuum chamber for adjusting the gas flow rate. A photograph of the valves for supplying gas is presented in Figure 4.7 (a). When a different gas is required for testing, the new gas cylinder must be added to the system. As presented in Figure 4.1, the inlet gas line combines with nitrogen from the microlab supply lines at the back in the vacuum pump room. To pump down the pressure in the chamber or vent a gas from the chamber, a bellows valve, presented in Figure 4.7 (b), is used. An illustration of a connection of gas supply plumbing is presented in Figure 4.8. The N_2 gas is used every test to pump up the pressure inside the bell-jar chamber. Especially, when a toxic gas is used, the N_2 gas is also used to purge residual toxic gas from the line and the chamber. As an example, the SO_2 cylinder and N_2 Gas Control Valves in the

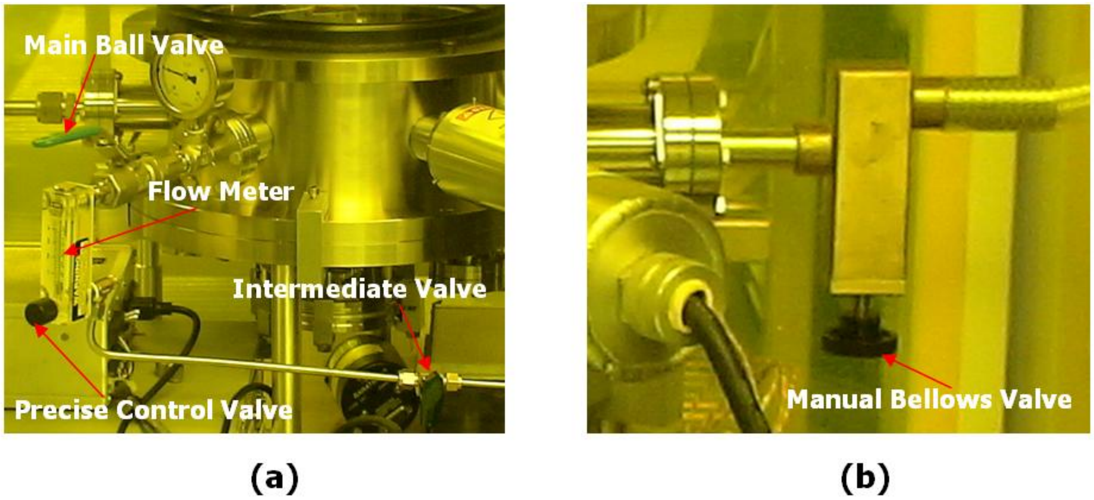

Figure 4.7: Valves of the MEMS Evaluation System: (a) Inlet Line Valves, (b) Outlet Line Valve

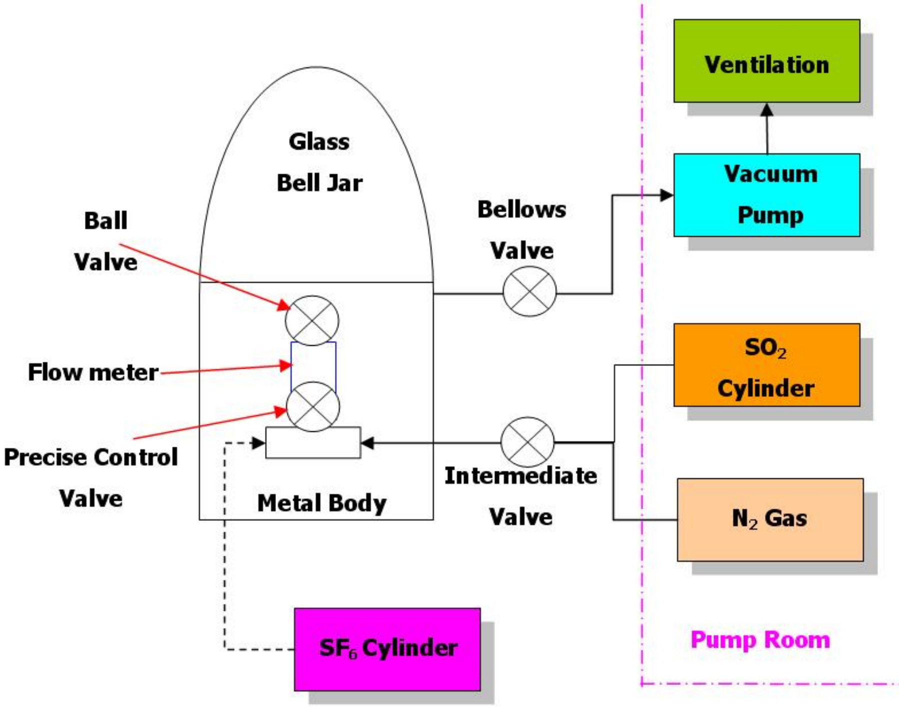

Figure 4.8: Illustration of Gas Plumbing

pump room are presented in Figure 4.9. A method to control SO_2 and N_2 Gas Valves is presented in Appendix A.2.

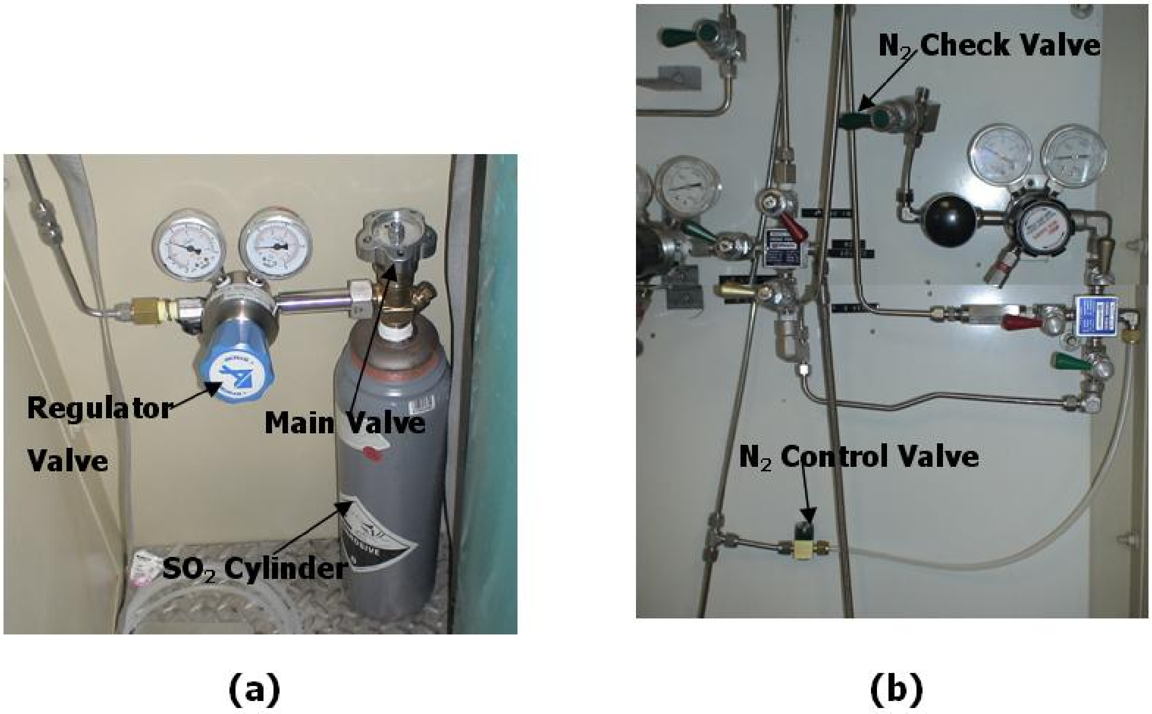

Figure 4.9: (a) SO_2 Cylinder and Valves (b) N_2 Gas Control Valves

4.4 Capabilities

The major components of the MEMS evaluation system consist of a bell-jar vacuum chamber, a small shaker, two laser displacement interferometers, and a dynamic analyzer. The capabilities of the components in the MEMS evaluation system of this study are presented below.

4.4.1 Bell-jar Vacuum Chamber

This vacuum chamber allows MDUT characterization over the pressure range of 50 mTorr to ambient. The pressure can be controlled with two hand valves, which are connected to the vacuum pump and the opened gas cylinder, respectively. The analog gauge provides a rough pressure reading and a combination of the pressure transducer and the digital readout allows the user to read the pressure at high resolution. The electrical feedthrough assembly is compatible with the D-sub 9-pin connector, which allows easy connection to the vacuum chamber. With the substrate quartz lamp below the plate, thermal evaluation can also be performed. The detailed specifications for the components of the bell-jar vacuum chamber are:

- Cover Material: Glass
- Chamber Lowest Pressure: 50 mTorr
- Electrical Feedthrough: 9-pin D-sub
- Heater Max. Temperature: 200°C
- Dynamic Range of Pressure Transducer: 0 to 1 Torr for 10V
- Digital Pressure Readout: 1 mTorr resolution
- Analog Pressure Guage: -30 to 200 psi
- Vacuum Pump: Mechanical Pump

4.4.2 Small Shaker

This shaker uses a electromagnetic field to induce sinusoidal motion with a frequency range of DC to 18kHz in the attached shaker head onto which the MDUT is mounted. A photograph of the Mini-shaker Type 4810, which is manufactured by B&K, is presented in Figure 4.10.

- Frequency Range: DC to 18 kHz

- Force Rating (peak): 2.25 lbf @65 Hz to 4 kHz, 1.5 lbf @ 65 Hz to 18 kHz

- Max. Bare Table Acceleration: 56 g

- Dimension: Diameter- 3 in, Height- 2.9 in

Figure 4.10: Photograph of the Mini-shaker Type 4810

4.4.3 Optical Measurement System

A photograph of an OFV-353 laser unit and an OFV-2610 vibrometer controller, manufactured by Polytec, is presented in Figure 4.11. The laser unit emits a single, visible laser to the object, and focusing can be adjusted with the lens housing. The laser unit also has a mirror allowing the placement of the laser spot to be manually adjusted. The unit has an adjustable measurement range of 20μm/V to 5120μm/V.

Figure 4.11: Optical Measurement System: (a) Vibrometer Controller, (b) Laser Unit

4.4.4 Dynamic Signal Analyzer

Figure 4.12 presents a photograph of the HP 35665 Dynamic Signal Analyzer. The analyzer can analyze two input signals with a maximum 800-line resolution and a 51.2kHz frequency bandwidth. The fast averaging function, over 12KHz in speed, is useful for viewing statistical graphs. The analyzer allows analysis in the time and frequency domains. The source output port provides various types of signals, such as sine, random, pink noise, and chirp signals, which can be used to control the power amplifier for the small shaker.

Figure 4.12: Photograph of the HP 35665 A Dynamic Signal Analyzer

CHAPTER 5

APPLICATION OF THE MEMS EVALUATION SYSTEM

To demonstrate the usefulness of this evaluation system, a multipurpose MEMS device was fabricated and utilized in a variety of tests involving this evaluation system. This micromachined device was used in several applications, including as a relative velocity sensor [35], as an active vibration isolator [45-46], and as a testbed for evaluating the performance of a MEMS device in different gas environments. In the relative velocity sensor application, the performance of the sensor was investigated by measuring the relative displacement and the relative velocity between a fixed electrode and a movable electrode while the device was excited by the electromechanical shaker in the evaluation system. The MEMS device was also used as a passive vibration isolator to evaluate the effects of packaging a MEMS device in different gas chemistries at various pressures, through measuring the effect on the mechanical quality factor of the device when excited by the shaker. This same device was then used in an active vibration isolator, which was evaluated in the system. Finally, the MEMS device was used as a capacitor structure for evaluating the relative permittivity of different gas chemistries at various pressures.

5.1 The MEMS Device

The MEMS device consisted of a micromachined Si square structure with a proof mass pad attached to a surrounding frame by eight springs. The frame and proof mass pad had a nominal thickness of 375μm. The spring thickness was set during microfabrication by the length of time the wafer was DRIE etched. The surrounding frame was 19.6mm long and 3.5mm across, and the center square proof mass pad was 10mm across. Each of the eight springs was 1300 μm long and

225 μm wide. 40μm was selected as the designed spring thickness, which resulted in a designed mechanical natural frequency of 1.39KHz. The design for this MEMS device had previously been used in other applications [47]. A photograph of the fabricated Si MEMS device is presented in Figure 5.1.

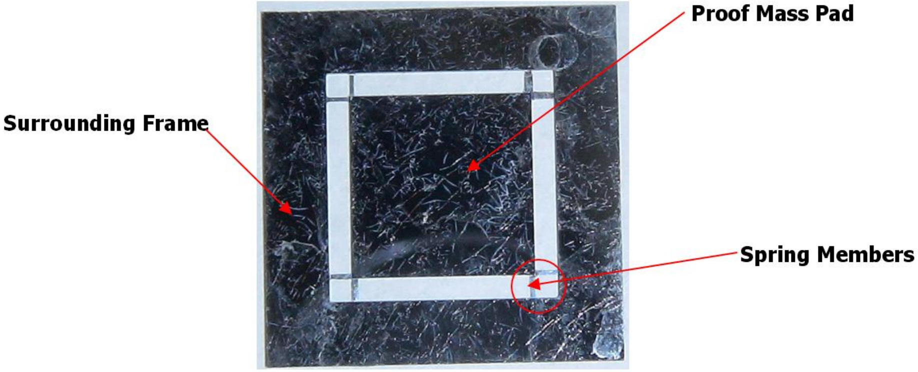

Figure 5.1: Si MEMS Structure

5.2 Fabrication of the MEMS Device

A detailed fabrication process traveler for fabricating the MEMS device is included in Appendix A.1.

I. Wafer & Mask:

A 375μm thick silicon double-side polished 4-inch wafer, with a resistivity of 1-10 Ω-cm, was utilized to fabricate the MEMS device. Since the feature size was relatively large, two laser photoplot masks were used to pattern the front and bask sides of the wafer. Seven devices were fabricated per wafer.

II. Cleaning:

There were several wafer cleaning steps used to get rid of contaminants and foreign materials from the surface of the wafer. First, the wafer was cleaned with a 50:1 H_2O:HF solution at room temperature to remove oxides from the wafer surface. To remove alkali metal and hydroxides, the wafer was soaked in a 6:1:1 solution of H_2O:HCL:H_2O_2 at 80°C for 10 min. Next, the wafer was rinsed and blow dried.

III. Dehydration & HMDS Deposition:

The wafer was cleaned with oxygen plasma in the Matrix etcher for 3 min. Then, the wafer was dehydrated in a dehydration chamber at 120°C for 20 min to remove moisture. Right after dehydration, the Hexamethyldisilazane (HMDS) deposition was performed in a HMDS chamber at ambient temperature for 5 min, after cleaning the inside of the chamber and then pouring 2 to 3 drops of HMDS into the chamber, which was used as an adhesion promoter.

IV. Top Side Photolithography:

Before patterning with a mask, Clarient 5214E photoresist was spun on at 1000 rpm for 30s, which resulted in a thickness of approximately 2.5 μm, and the wafer was then softbaked on a hotplate at 108°C for 2 min. Mask exposure was performed in the MABA 6 aligner using two 10s exposures. Finally, the wafer was developed in a 2:1 solution of water:AZ 400K developer. It took more than 30s to develop the wafer. If there had been residual photoresist on the pattern even after 30s of developing, additional developing was performed in 30s intervals, followed by microscopic inspection, until the remaining photoresist was removed.

V. Top Side DRIE Etching & Photoresist Strip:

As the spring thickness was designed to be 40μm, the wafer was etched in the STS ASE DRIE etcher with frequent inspections to meet the 40μm depth as close as possible. After etching was completed, the wafer was placed in the Matrix for 5 min to strip the remaining photoresist.

VI. Bottom Side Photolithography:

The bottom side photolithography was very similar to the top side photolithograpy process, except for the photoresist, the mask, and related parameters. After a 3 min descum in the Matrix and a 5 min HMDS deposition, Clarient 4620 photoresist was spun on at 1000rpm for 30s. Then a 108°C 2min softbake was followed by a 60s exposure using the bottom mask in the MABA 6 aligner. In this step, the pattern on the top side of the wafer was aligned to the bottom side mask using cross alignment marks on both sides. The exposed wafer was developed in a developer with the same ratio as used in the top side photolithography, and then finally hardbaked at 120°C for 2 min on a hotplate.

VII. Bottom Side DRIE Etching:

The bottom side of the wafer was DRIE etched until the depth reached 140μm, which was enough to cleave the wafer.

VIII. Wafer Cleaving:

Once the DRIE etching was finished, the outer square patterns on the bottom side were extended by scratching with a diamond cutter. The wafer was then cleaved very carefully along the extended scratch lines.

IX. DIE Mounting;

To complete the etching, each cleaved die were attached to a Si wafer. Clarient 4620 photoresist was used as an adhesive. It was spun on at 1500 rpm for 30s, and then the wafer was softbaked on the hotplate at 108°C for 2 min.

X. Bottom Side DRIE Etching:

To complete the DRIE etching that removes the remaining 170μm of Si, the wafer is placed back in the STS ASE and further etched in DRIE machine. Checking often to prevent over etching, the DRIE etching was continued until the red photoresist was seen using a microscope.

XI. Post DRIE MEMS Die Removal & Cleaning:

The wafer and die were soaked in acetone until they separated. After separation, first, a wiper tissue was soaked in isopropyl alcohol, and then the die was placed on the tissue for 30s. The wiper tissue was used to take the die out instead of using tweezers.

XII. E-Beam Metallization:

The top side of the die was then metalized with titanium (Ti) and gold (Au) by E-beam evaporation, after taping the four corners of the die to a clean wafer using Kapton tape.

5.3 Background for a Micromachined Parallel Plate Capacitor Structure [46]

- Mechanical and Electro Dynamics:

An illustration of a two parallel electrode MEMS structure, where the bottom electrode is fixed and the top electrode can move up and down relative to the bottom electrode, is presented in Figure 5.2.

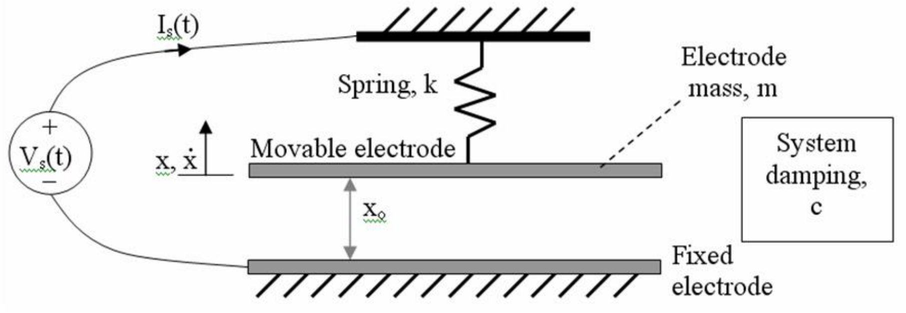

Figure 5.2: Parallel Electrode Structure[46]

For this type of structure, the equation for transmissibility is:

$$|T(j\omega)| = \frac{\sqrt{(\frac{\omega_n\omega}{Q})^2 + \omega_n^4}}{\sqrt{(\omega_n^2 - \omega^2)^2 + (\frac{\omega_n\omega}{Q})^2}} \tag{5.1}$$

Where |T(jw)| is the transmissibility, Q is the mechanical quality factor, ω_n is the natural frequency of the system, where:

$$\omega_n = \sqrt{\frac{k}{m}} \tag{5.2}$$

and

$$Q = \frac{\sqrt{km}}{c} \tag{5.3}$$

Since most MEMS devices have Q values greater than five, |T(jω)| has a high resonant peak at approximately ω_n.

- Current Flow into the MEMS Capacitor:

Let the relative electrode motion by modeled by:

$$x(t) = x_A sin(\omega t) \tag{5.4}$$

and the resulting capacitance between the parallel electrodes can be modeled as:

$$C_s(t) = \frac{\varepsilon_o \varepsilon_r A}{x_o + x_A sin(\omega t)} \tag{5.5}$$

where $\varepsilon_o \varepsilon_r$ is the permittivity of the dielectric material between the two electrodes, A is the overlapping electrode area, x_o is the rest distance, x_A is the amplitude of the sinusoidal relative motion with frequency ω_n. This model for the capacitance ignores fringing, which is usually small if the electrode area is much larger than the separation distance. If a small voltage, V_s(t), which is less than the pull-in voltage, is applied across the two electrodes, then charge, q(t), accumulates in the time varying capacitor, C_s(t), according to:

$$q(t) = C_s(t) V_s(t) \tag{5.6}$$

The current flowing into the capacitor, $I_s(t)$ can then be obtained by taking the derivative of q(t), resulting in

$$I_s(t) = C_s(t) \frac{dV(t)}{dt} + V_s(t) \frac{dC_s(t)}{dt} \tag{5.7}$$

Suppose that V$_s$(t) is constrained to be a small, constant DC voltage, V$_b$. Therefore the current flowing into C$_s$(t) becomes

$$I_s(t) = V_b \frac{dC_s(t)}{dt} = -\frac{V_b \varepsilon_o \varepsilon_r A x_A \omega cos(\omega t)}{(x_o + x_A sin(\omega t))^2} \tag{5.8}$$

The negative sign in the numerator indicates that current flows out of the capacitor when the distance between the two electrodes is increasing, which is correct since the capacitance is decreasing. Likewise, when the distance between the electrodes is decreasing, capacitance is increasing, resulting in current flow into the capacitor and a positive value for I$_s$(t). For x_o/x_A having a large ratio,

$$I_s(t) \cong -\frac{V_b \varepsilon_o \varepsilon_r A x_A \omega cos(\omega t)}{x_o} \tag{5.9}$$

and that the relative velocity between the electrodes is

$$\dot{x}(t) = x_A \omega cos(\omega t). \tag{5.10}$$

If x_o/x_A is small, (5.9) is not a valid approximation for I$_s$(t). However the polarity of I$_s$(t) correctly identifies the direction of relative velocity.

5.4 Relative Velocity Sensor in Low Pressure Environment

The relative velocity sensor was evaluated in the evaluation system at ambient and low pressure.

- Assembly

The micromachined Si structure was assembled with exactly the same parts as for the closed-loop damping control testing except for the PCB board, which is discussed in detail in the closed-loop damping control section. The PCB board used in this test had a micromachined capacitor interface circuit consisting of a transimpedance amplifier and a two stage voltage amplifier on the front side and bottom electrodes on the back side.

- Micromachined Capacitor Interface Circuit

A schematic diagram of the capacitor interface circuit is presented in Figure 5.3. The first stage, a transimpedance amplifier (TIA) with a gain of -100,000Ω, converted the current flowing into the sensor capacitor into a voltage signal. Then, a two stage amplifier consisting of an inverting amplifier and an non-inverting amplifier, with a combined gain of -10100V/V, were used to amplify the TIA output voltage to a reasonable level for recording the data.

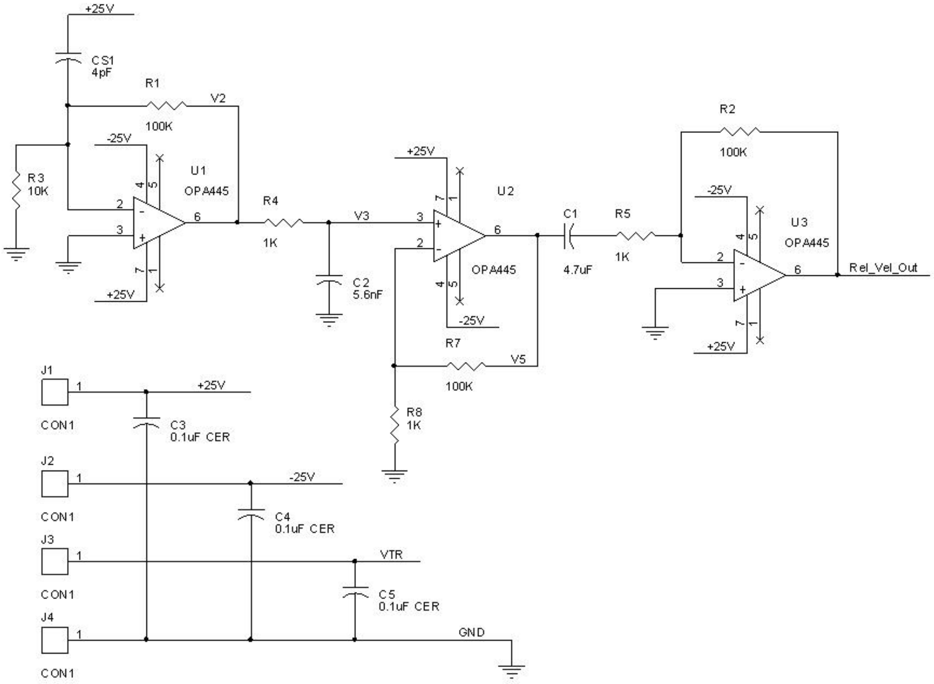

Figure 5.3: Schematic Diagram of Capacitor Interface Circuit

- Testing

The velocity sensor assembly with the capacitor interface circuit was mounted on the small shaker inside the MEMS evaluation system. The resonant frequency of the velocity sensor was investigated first using a wide bandwidth random vibration excitation. A time trace of the velocity sensor at the resonant frequency was recorded with the signal analyzer by detecting the relative displacement with two interferometers. This experiment to test the relative velocity sensor was performed at ambient pressure and at low pressure (approximately 0.2 Torr). Time traces of the relative displacement between the two electrodes, measured using the interferometers, and the output signal from the sensor board are presented in Figure 5.4 (ambient pressure test) and Figure 5.5 (low pressure test). As would be expected for a sinusoidal displacement, the relative velocity sensor's output

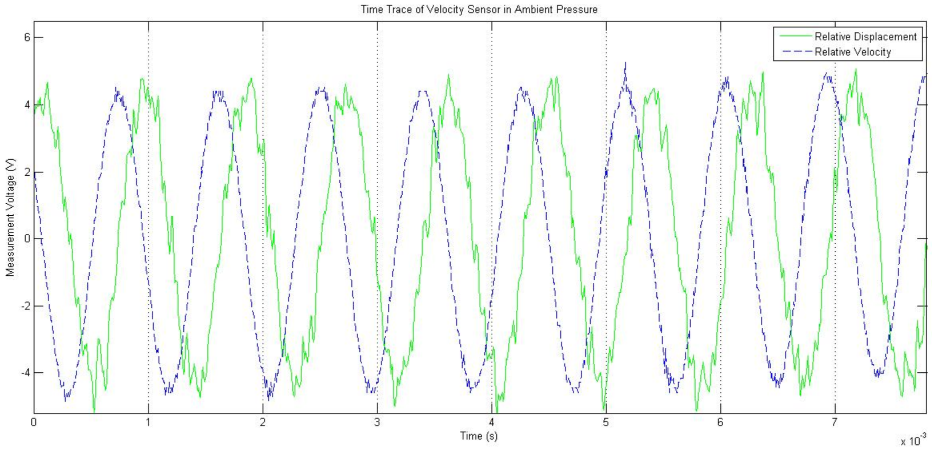

Figure 5.4: Time Traces of the Measured Relative Electrode Displacement and the Sensor Output at Ambient Pressure

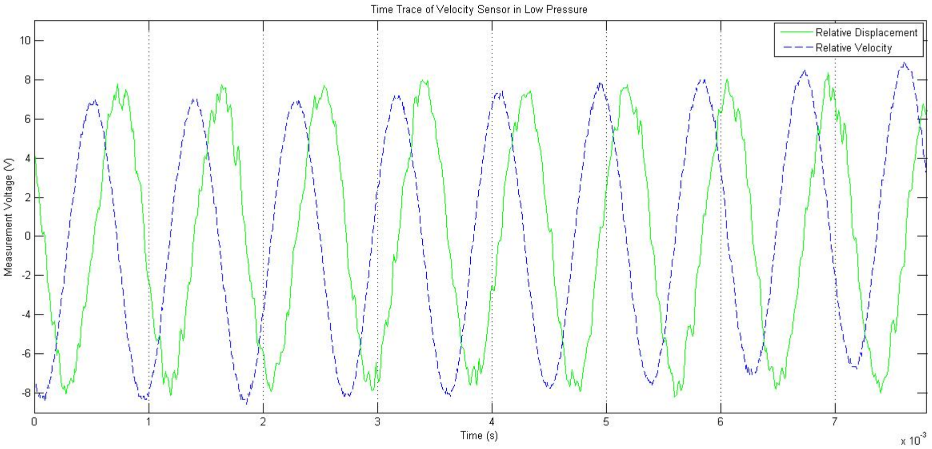

Figure 5.5: Time Traces of the Measured Relative Electrode Displacement and the Sensor Output at Low Pressure

signal is also sinusoidal and leads the displacement waveform by 90 degrees. Much of the noise in the relative velocity signal is due to the differentiation of the noise in the relative displacement signal.

This test was performed primarily to verify the operation of the MEMS evaluation system. Also, since the relative velocity sensor is a key component of the closed-loop damping controller, it was important to verify that the small shaker in the system was powerful enough to generate sufficient relative motion between the device's electrode to measure the relative velocity.

5.5 Closed-loop Damping Control At Low Pressure[45]

A closed-loop damping control system was evaluated using the MEMS evaluation system.

- Assembly:

The backside of the proof mass was the upper or movable electrode. The micromachined Si structure was mounted onto the back side of a double layer printed circuit board directly over a planar electrode, the fixed electrode, using a nonconductive spacer with a nominal thickness of 100μm, which set the rest distance between the two electrodes. The feedback controller PCB, a photograph of which is presented in Figure 5.6, was integrated with the micromachined Si structure as the top electrode for several evaluations. A photograph and an illustration of the assembled MEMS device are presented in Figure 5.7. The parallel plate actuator (PPA) and the sensor bottom electrode are on the feedback control circuit PCB. The small round center sensor electrode was used to detect the relative velocity and the donut shaped outer electrode acted as the PPA bottom electrode and connected to the feedback controller circuit.

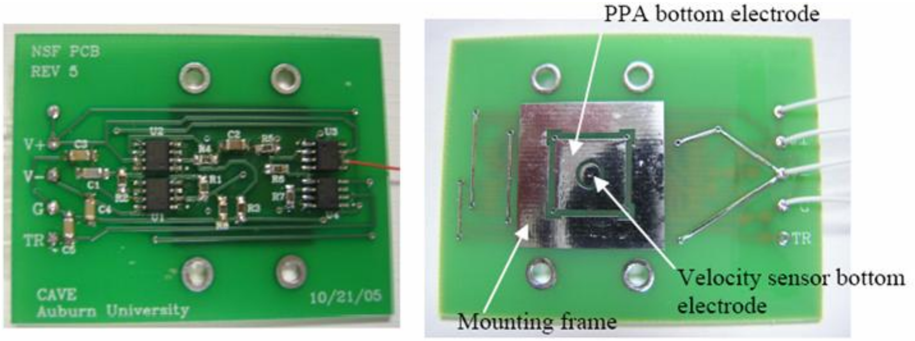

(a) (b)

Figure 5.6: Feedback Controller Circuit Board [45]: (a) Front side, (b) Back side

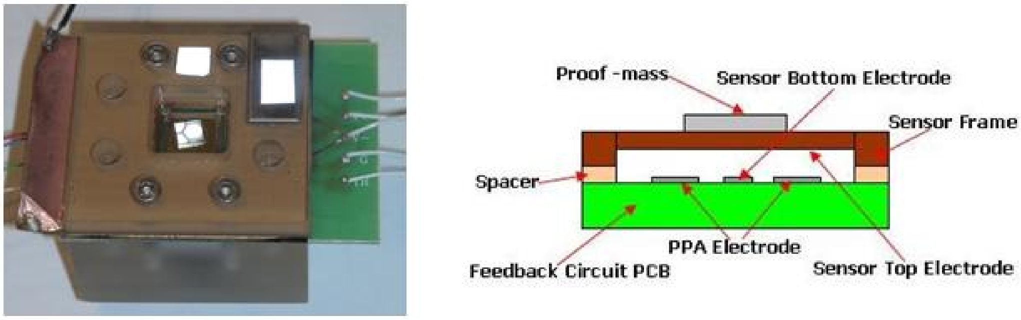

(a) (b)

Figure 5.7: MEMS Device with the Feedback Controller PCB: (a) Assembled MDUT with the Feedback Controller Circuit PCB, (b) Illustration of the side view of an assembled MDUT [45]

- Feedback Controller Circuit:

The feedback controller electronics circuit consisted of a low impedance op amp current to voltage conversion circuit (transimpedance amplifier), a two stage voltage amplifier and a voltage comparator. The output of the comparator powered a PPA, which was used to increases the mechanical damping of the active isolator. A schematic diagram of the feedback controller circuit is presented in Figure 5.8. CS1 represented the velocity sensor capacitance and CX1 the PPA capacitance. When the upper electrode was moving toward the bottom electrodes, the sense capacitance was increasing in size, resulting in current flow into the sense capacitor. This resulted in a positive voltage being applied to the comparator's noninverting input and +25V on the comparator output being applied to the bottom PPA electrode. With the top electrode hardwired to +25V, both PPA electrodes had the same potential and no electrostatic force was generated. Therefore the PPA was off whenever the top electrode was moving toward the bottom electrodes. When the upper electrode moved away from the bottom electrodes, the sense capacitor decreased in size, resulting in current flow out of the sense capacitor. This resulted in a negative voltage being applied to the comparator's noninverting input and -25V on the comparator output being applied to the bottom PPA electrode. Since the top electrode was hardwired to +25V, the PPA electrodes had a 50V potential difference, which resulted in the generation of an electrostatic force that attempted to retard the separating motion of the upper and bottom electrodes. As soon as the electrodes quit moving away from each other, the PPA shut off. The net result was that kinetic energy was removed from the oscillating mechanical system, resulting in an increase in mechanical damping.

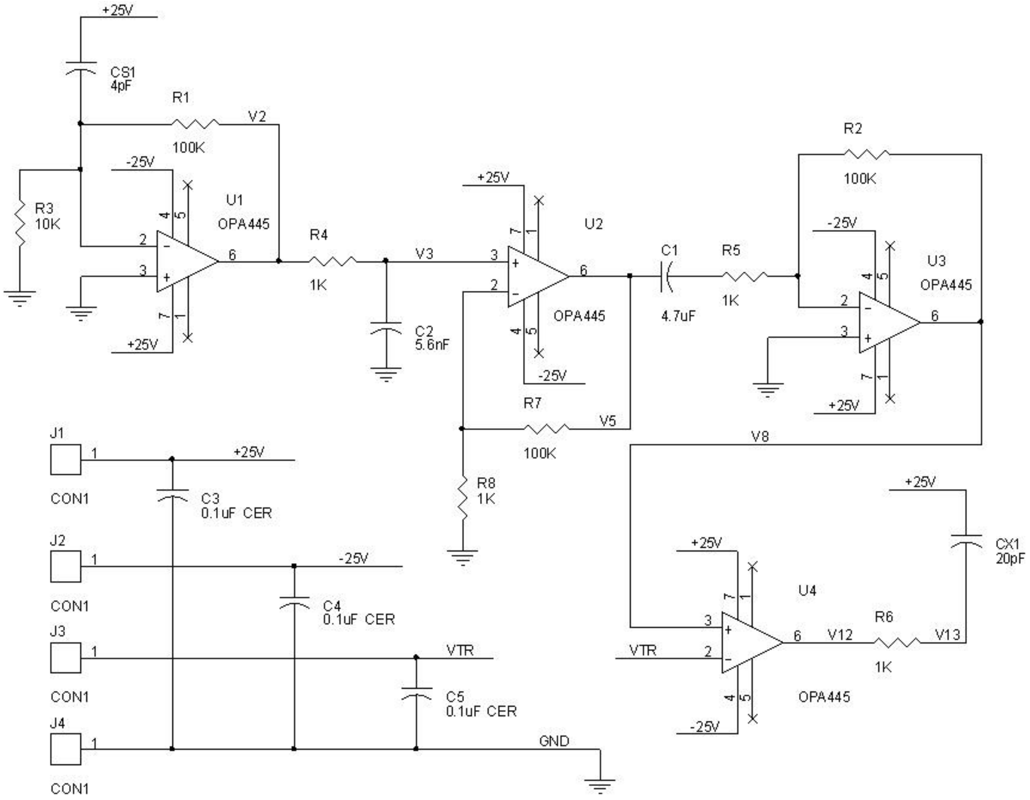

Figure 5.8: The Schematic Diagram of the Feedback Controller Circuit[45]

• Testing:

To evaluate the closed loop system, the assembled MEMS device was placed in the chamber and evaluated at low pressure. Using the electromagnetic shaker, the device was vibrated with and without the control loop activated. For the closed loop tests, the comparator trip voltage, VTR, was tied to ground. The feedback controller circuit could lower the quality factor in low pressure, and the results of this test are presented in Figures 5.9. The data shows that Q decreased a large amount with the controller activated, from approximately 138 to 50, when the device was tested at 50 mTorr pressure. Observe that the plot in Figure 5.9 shows a shift in the resonant frequency of approximately 100Hz when the controller is activated. It is speculated that the change in the resonant frequency is due to an increase in the system spring constant due to the nonlinearity in the double clamped spring system when the biased controller electrodes result in a nonzero average proofmass displacement.

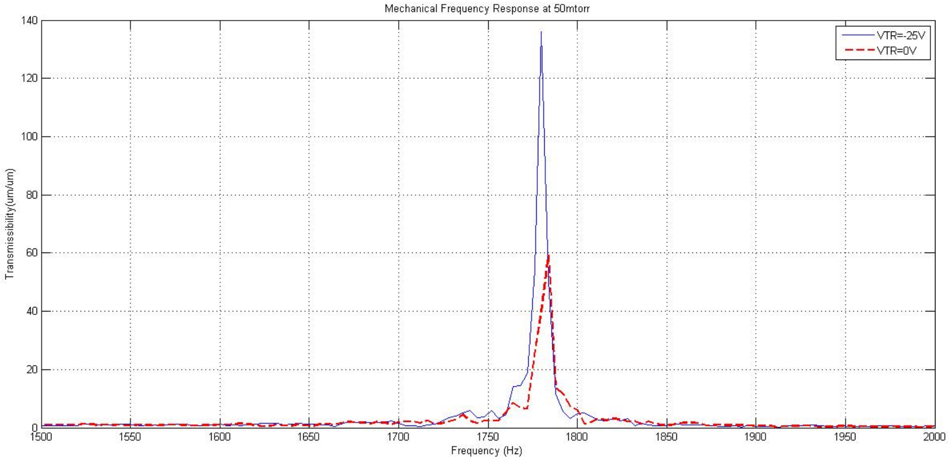

Figure 5.9: Mechanical Frequency Responses Due to Feedback Control Signal at Low Pressure

5.6 Electrostatic Enhancement of MEMS Devices

In this test, the effects of packaging an electrostatic MEMS device in a gas with a relatively high dielectric constant were investigated. The MEMS test article was the same micromachined Si device used in the other tests. It was attached to a PCB having a single large electrode, just like the relative velocity sensor was assembled. The capacitance between the two electrodes was then measured in different gas chemistries at various pressures. A photograph of the bottom electrode of the PCB is presented in Figure 5.10.

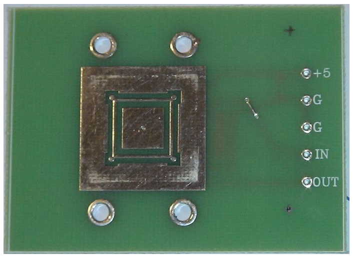

Figure 5.10: Bottom Electrode of the Test PCB

For this test, the MEMS device's capacitance was measured in air, N_2, SO_2, SF_6, and water vapor using a model LCR-821 LCR meter, manufactured by GW Instek. A photograph of the LCR-821 is presented in Figure 5.11.

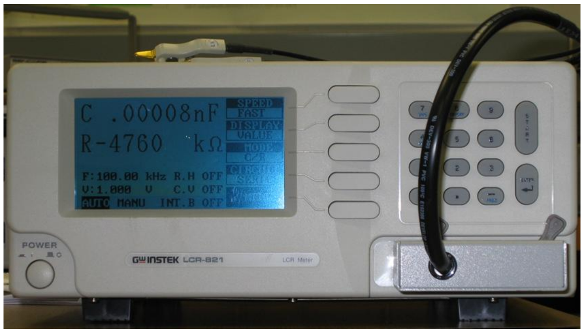

Figure 5.11: Photograph of GW Instek LCR-821

The purpose of these tests were to investigate if the packaging of an electrostatic MEMS device in various gas environments could be used to enhance performance either by using a gas with a high relative permittivity or through effecting the system mechanical quality factor. The relevant physical properties for air, N_2, SO_2, SF_6, and water vapor are presented in Table 5.1. The density properties were calculated by

$$\rho = \frac{P}{RT} \tag{5.11}$$

where R=8.314472(J/K·mol).

The permittivity of water vapor was calculated with

$$\varepsilon = 1 + \frac{\rho(3aT + 3b)}{T} \tag{5.12}$$

where 3b=3449 and 3a=0.671 [49].

Table 5.1: Viscosity, Density, and Permittivity for Air, N_2, SO_2, SF_6, and Water Vapor [48-49]

Gas	Viscosity(μPa ·s) @27°C, 100kPa	Density(Kg/m^3) @25°C, 1atm	Dielectric Constant @20°C, 1atm
Air	18.6	1.1845	1.0005364
N_2	17.9	1.1458	1.0005480
SO_2	12.9	2.6195	1.0082500
SF_6	15.3	5.9738	1.0020000
Water Vapor	9.7	0.7369	10.181060

The measured capacitance values in various gases at different pressures are presented in Table 5.2. The capacitance values decrease as the pressure decreases for each gas chemistry. It was not meaningful to compare absolute capacitance values to each other as the calibration of the probes of the LCR meter had a big discrepancy between tests. When the absolute capacitance values of the results were compared separately, as presented in Figure 5.12 and Figure 5.13, the magnitude

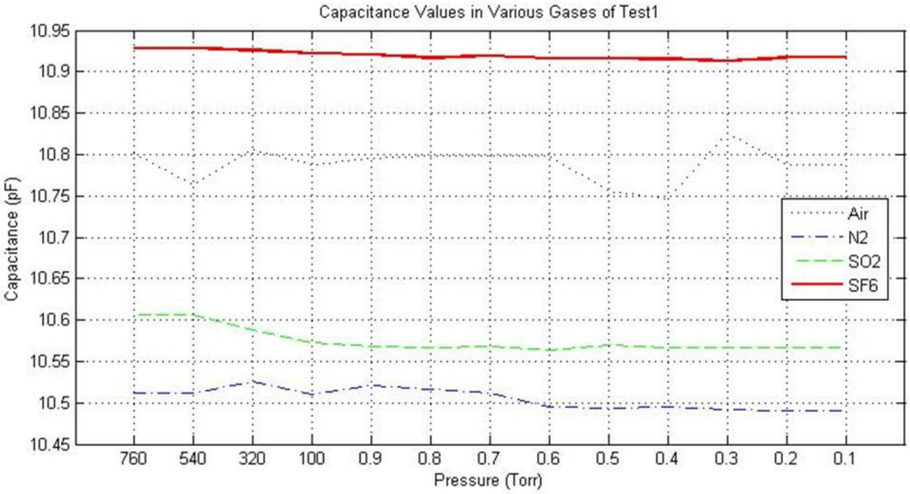

Figure 5.12: Capacitance Change in Test1

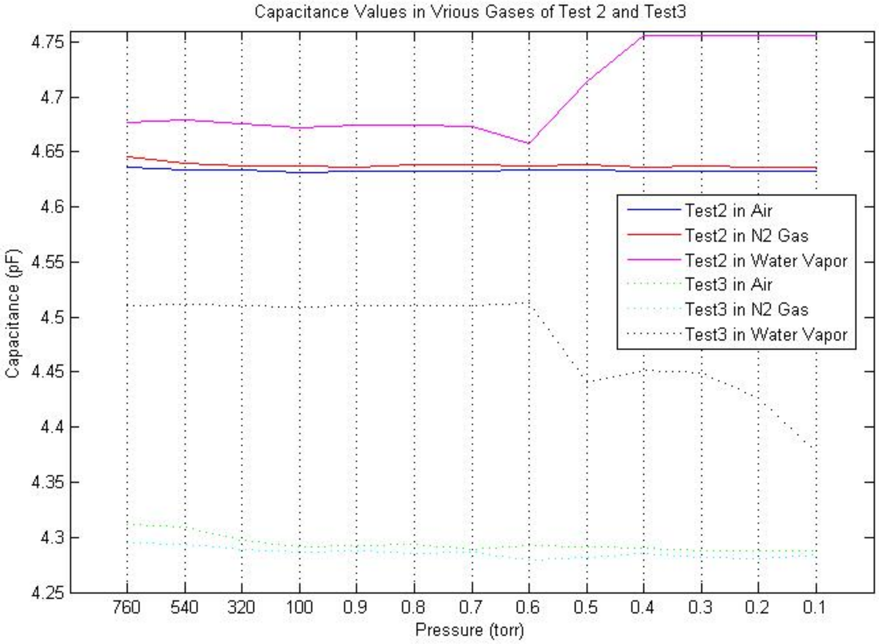

Figure 5.13: Capacitance Change in Test2 and Test3

of the measured capacitance for each gas compared well with the magnitude of the dielectric constants for each gas, except for SF_6 in Test1 and air in Test3. However, when the difference of the capacitances between the lowest and the highest pressure were compared to eliminate the calibration errors, instead of comparing absolute capacitance values, the capacitance difference is proportional to the gas permittivity, except for the air. The reason for this was speculated to be that the air was not dry air. Water vapor has a high relative permittivity, and it is thought that water vapor in the air injected into the system, or from water molecules that liberated from surfaces in the chamber, affected the capacitance measurement. In order to perform this test, the gases except for water vapor were injected into the chamber, while water vapor was evaporated from water in a plastic bottle inside the chamber for the test. This method to fill the chamber with water vapor was problematic, because the liquid water in the plastic container would freeze as the pressure was lowered. Therefore for water vapor, the capacitance was measured while the pressure was deceasing, unlike with the other gases. As a result of these tests, it was concluded that hermetically packaging an electrostatic MEMS device in a low pressure high dielectric constant gas would not significantly enhance the device's performance.

Table 5.2: Capacitance under Various Gases at Different Pressures

Pressure	Air			N_2			SO_2	SF_6	w. vapor
(Torr)	Test1	Test2	Test3	Test1	Test2	Test3	Test1	Test1	Test3
760	10.802	4.6361	4.3115	-	-	-	-	-	-
540	10.764	4.6342	4.3088	10.512	4.6391	4.2938	10.607	10.928	4.5110
320	10.806	4.6338	4.2975	10.526	4.6378	4.2893	10.588	10.926	4.5100
100	10.787	4.6319	4.2918	10.510	4.6370	4.2862	10.573	10.922	4.5088
0.9	10.795	4.6328	4.2923	10.521	4.6364	4.2872	10.568	10.921	4.5104
0.8	10.799	4.6320	4.2932	10.517	4.6389	4.2857	10.566	10.917	4.5101
0.7	10.798	4.6325	4.2891	10.511	4.6385	4.2860	10.568	10.919	4.5099
0.6	10.799	4.6337	4.2925	10.495	4.6374	4.2793	10.564	10.916	4.5123
0.5	10.755	4.6332	4.2918	10.493	4.6385	4.2823	10.570	10.916	4.4409
0.4	10.746	4.6330	4.2897	10.495	4.6362	4.2849	10.566	10.915	4.4514
0.3	10.826	4.6321	4.2883	10.492	4.6373	4.2817	10.567	10.913	4.4495
0.2	10.788	4.6325	4.2880	10.491	4.6365	4.2810	10.566	10.917	4.4269
0.1	-	4.6321	4.2879	-	4.6365	4.2846	10.566	-	4.3775
C_{maxp}-C_{minp}	0.014	0.0040	0.0236	0.021	0.0026	0.0092	0.041	0.011	0.1335
$C_{average}$	0.014867			0.01093			0.041	0.011	0.1335

5.7 Transmissibility vs. Pressure in Various Gases

These tests were performed to investigate the effect on mechanical damping of a MEMS device by packaging it in various gas chemistries at pressures equal to or lower than ambient pressure. The same gases were evaluated here as were evaluated in the electrostatic enhancement of MEMS devices tests. The various gases were evaluated at these pressures: every 220 Torr from 760 Torr to 100 Torr and every 0.1 Torr from 0.9 Torr to 0.2 Torr. The theoretical mechanical frequency response indicates that the Q values at each testing pressure should increase as the pressure deceases and as the gas viscosity decreases. The viscosity at 25°C and the density at 25°C, at 1atm for each gas in Table 5.1 is as follows; Air- 18.5 μPa $\cdot$s and 1.19 kg/m^3, SF_6- 15.3 μPa $\cdot$s and 6.1 kg/m^3, N_2- 17.9 μPa $\cdot$s and 1.14 kg/m^3, water vapor- 9.7 μPa $\cdot$s and 0.7369 kg/m^3

Measuring the transmissibility yields information regarding the type of response: lowpass, bandpass, or highpass frequency response, and its resonant frequency or frequencies and the mechanical quality factor, Q. The measurement of the quality factor reveals both the susceptibility of the device to ringing at its resonant frequency and what the time response will be to a step input.

Detailed mechanical frequency response results for each gases are presented in Figures 5.14 through 5.18, and mechanical frequency response results for each test are presented in Figures 5.19 through 5.22. The measured quality factors for all the tests are presented in the Table 5.3. The results showed that as the pressure decreased, the Q value increased, and the resonant frequency was substantially shifting to higher values. It is speculated that the gas adds a term to the system mass due to the gas having to be displaced by the motion of the vibrating proof mass. As the pressure decreases, the mass term would then decrease, thus increasing the resonant frequency of the device. The ambient pressure test with SF_6, SO_2, N_2, and water vapor was not performed, because it was difficult to keep the vacuum chamber at ambient pressure while supplying a pressurized gas to the bell jar. Even though transmissibility tests in ambient pressure with SF_6, SO_2, N_2, and water vapor could not been performed, when comparing the average quality factor values at pressures between 760 Torr and 100 Torr in Table 5.3, SF_6 gas resulted in the lowest quality factor. The order of average measured quality factors in this pressure range is exactly the reverse order of each gases' density factor. This results indicate that gas density is a more critical factor than the viscosity at the higher end of the pressures evaluated in this study: the lower the density, the higher the Q (order of density at 25°C, 1atm: $SF_6 > SO_2 >$ Air $> N_2 >$ water vapor). As presented in Figures 5.14 through 5.18, the quality factor commonly increased as the pressure decreased.

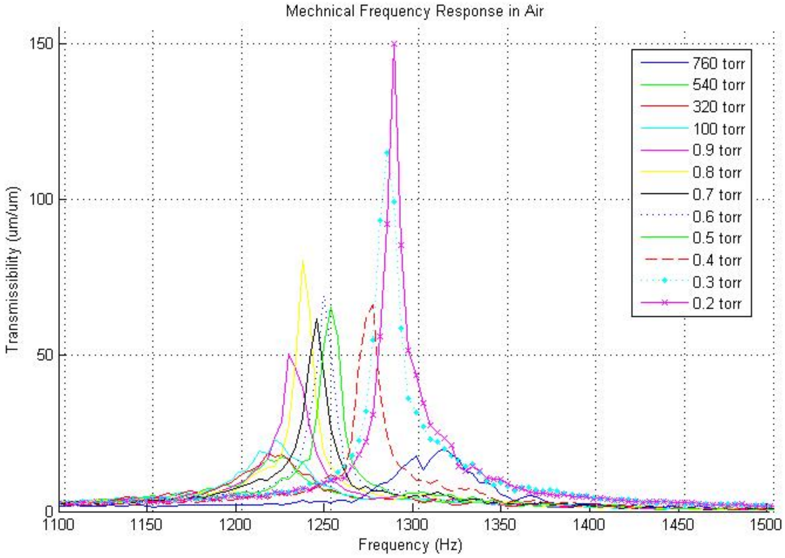

Figure 5.14: Mechanical Frequency Response in Air

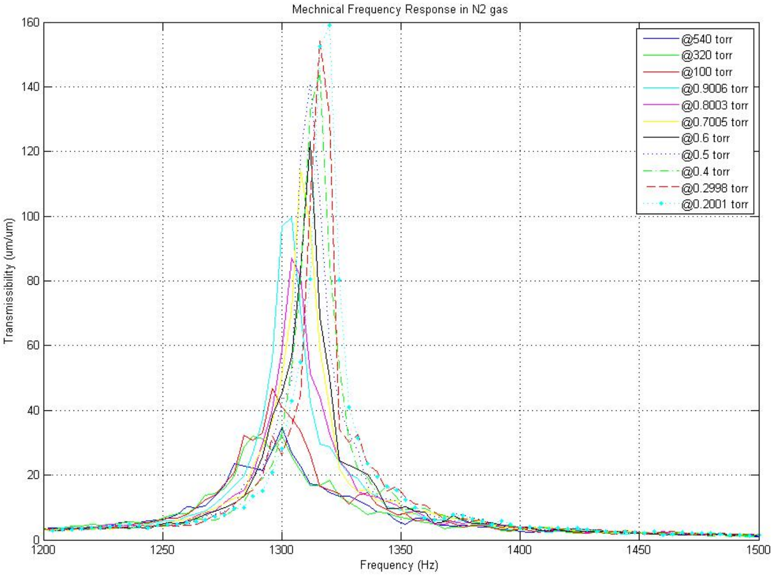

Figure 5.15: Mechanical Frequency Response in N_2

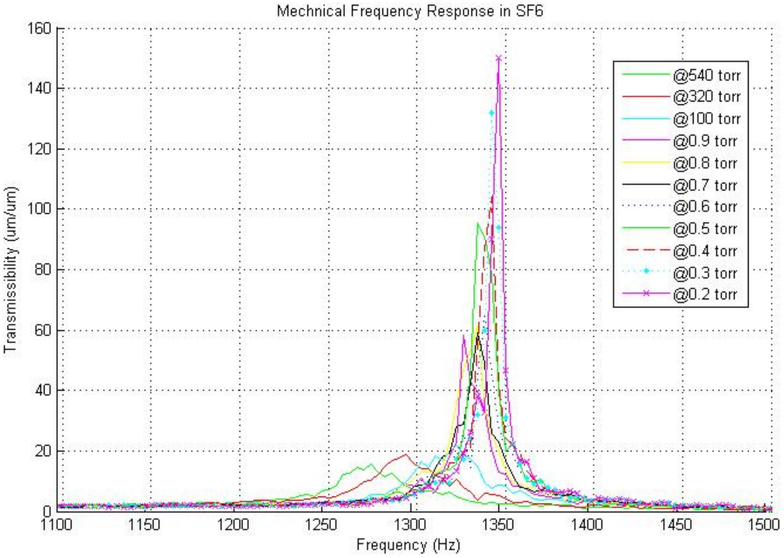

Figure 5.16: Mechanical Frequency Response in SF_6

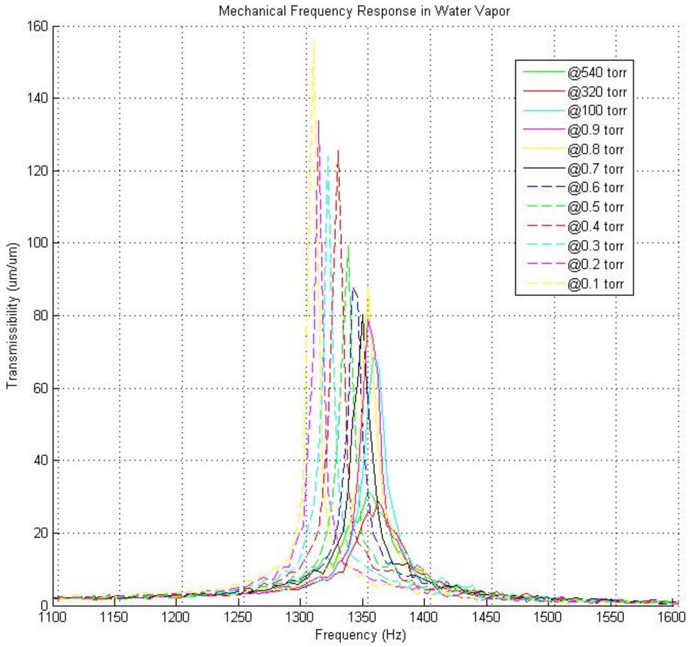

Figure 5.17: Mechanical Frequency Response in Water Vapor

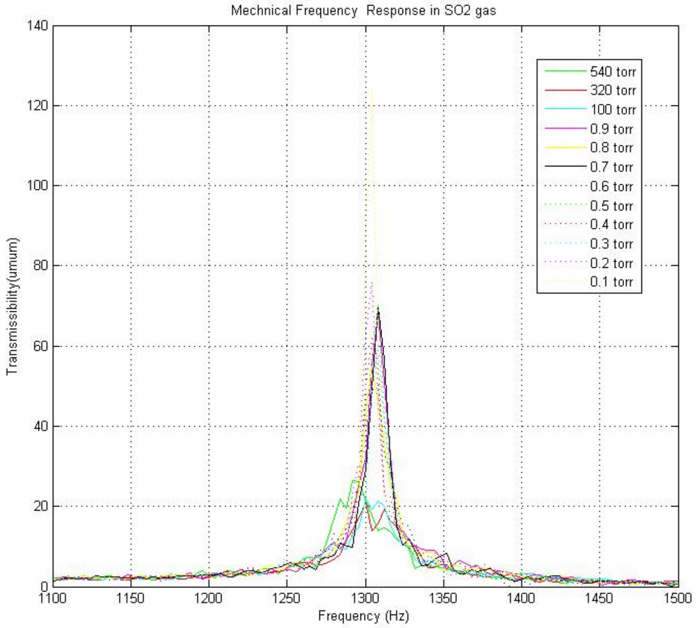

Figure 5.18: Mechanical Frequency Response in SO_2

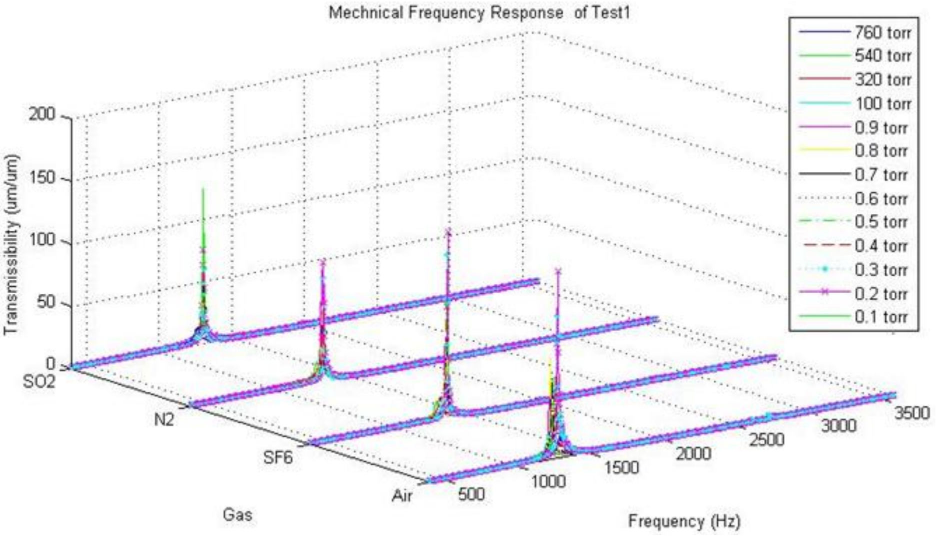

Figure 5.19: Mechanical Frequency Response in Various Gases and Pressures of Test1

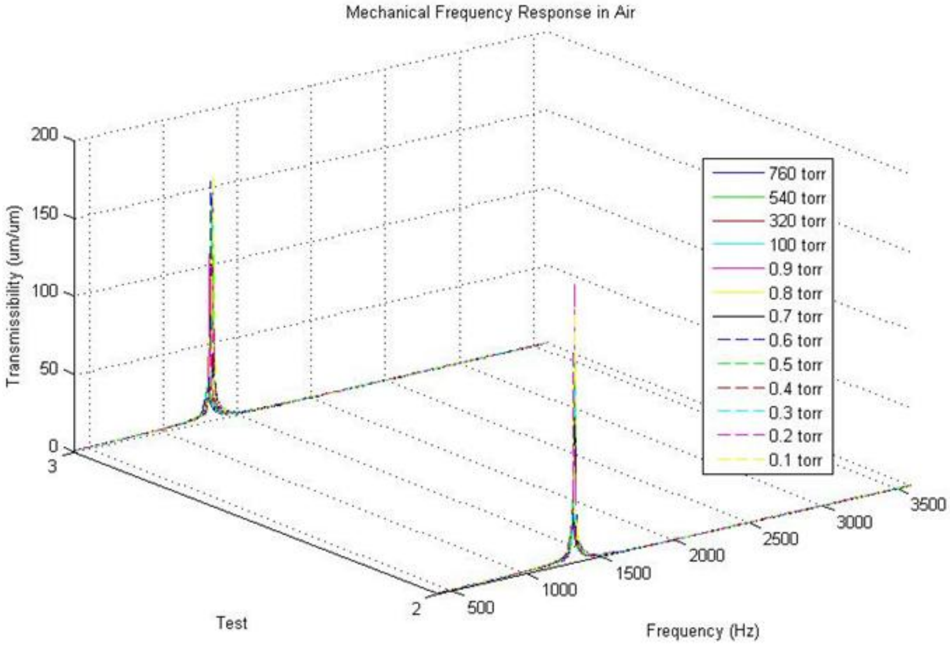

Figure 5.20: Mechanical Frequency Response in Air

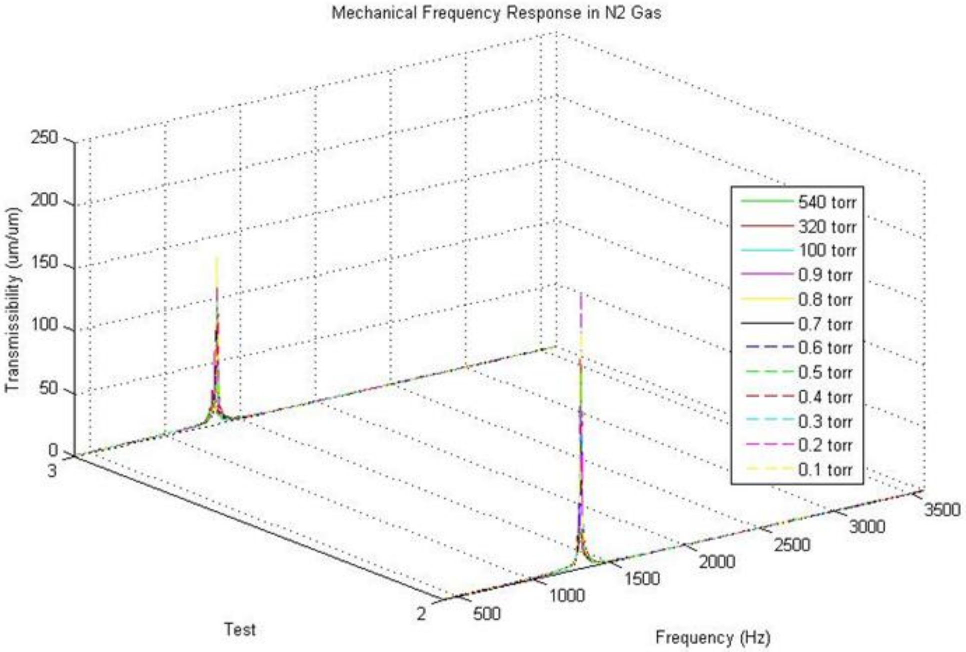

Figure 5.21: Mechanical Frequency Response in Nitrogen Gas

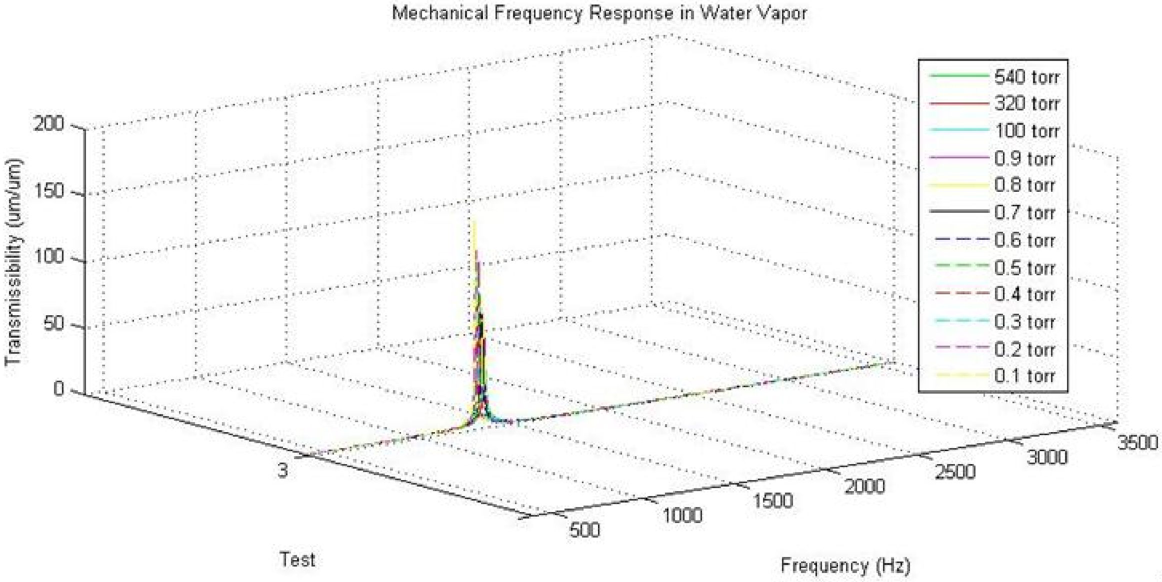

Figure 5.22: Mechanical Frequency Response in Water Vapor

Table 5.3: Quality (Q) Factor under Air and N_2 gas at Different Pressures

Pressure		Air			N_2	
(Torr)	Test1	Test2	Test3	Test1	Test2	Test3
760	20.2@1.316	27.7@1.324	20.4@1.296	-	-	-
540	17.6@1.224	26.1@1.308	28.0@1.300	17.1@1.264	27.9@1.316	21.6@1.320
320	18.4@1.216	27.0@1.316	26.4@1.300	23.8@1.288	29.6@1.312	27.0@1.320
100	23.0@1.220	29.7@1.320	34.4@1.304	22.0@1.288	34.0@1.304	29.4@1.328
Avg. Q		24.9			25.8	
0.9	50.4@1.228	72.7@1.320	107.3@1.312	89.5@1.300	124.7@1.312	68.0@1.332
0.8	80.6@1.236	83.6@1.324	104.6@1.316	61.7@1.300	94.2@1.312	78.3@1.336
0.7	61.7@1.244	113.4@1.324	111.9@1.320	61.4@1.300	113.8@1.312	74.7@1.336
0.6	69.1@1.248	111.5@1.320	154.0@1.320	69.0@1.304	108.9@1.312	81.8@1.340
0.5	65.4@1.252	146.5@1.320	139.2@1.328	59.0@1.304	156.0@1.308	90.2@1.340
0.4	66.1@1.276	114.0@1.320	137.5@1.328	64.7@1.308	169.1@1.308	109.0@1.344
0.3	115.0@1.284	149.7@1.324	145.3@1.328	83.8@1.308	133.6@1.312	105.6@1.344
0.2	149.9@1.288	179.4@1.324	150.1@1.332	95.6@1.312	219.5@1.308	118.4@1.348
0.1	-	170.0@1.324	156.3@1.332	-	190.3@1.308	134.1@1.344

Table 5.4: Quality (Q) Factor under SO_2, SF_6, and Water Vapor at Different Pressures

Pressure (Torr)	SO_2 Test1	SF_6 Test1	w. vapor Test3
760	-	-	-
540	26.5@1.292	15.7@1.276	28.8@1.348
320	21.2@1.300	18.7@1.296	31.6@1.352
100	21.8@1.300	21.7@1.324	28.8@1.360
Avg. Q	23.2	18.7	29.7
0.9	68.3@1.308	58.3@1.328	68.4@1.356
0.8	54.9@1.304	61.6@1.336	79.2@1.352
0.7	69.5@1.308	59.1@1.336	87.8@1.352
0.6	50.3@1.308	65.8@1.340	80.3@1.348
0.5	70.4@1.308	95.5@1.336	87.9@1.340
0.4	62.0@1.304	104.0@1.344	99.3@1.336
0.3	60.1@1.308	131.9@1.344	125.5@1.328
0.2	76.0@1.304	150.2@1.348	124.0@1.320
0.1	124.1@1.304	-	133.9@1.312

CHAPTER 6

CONCLUSIONS

In this thesis, the MEMS evaluation system and its application have been discussed. The evaluation system was designed and constructed for the mechanical and electrical characterization of unpackaged MEMS die and was used to measure the mechanical frequency response, the capacitance, and the behavior of closed-loop damping control, at various pressures in different gases. Current research efforts in MEMS evaluation system development show how such a system can be useful for testing MEMS die. The evaluation system provides practical mechanical and electrical characterization data on the MEMS device, which can be useful for design modification during the device development stage.

The test results for the closed-loop damping control system at low pressure showed that damping by the feedback control circuit reduced the quality factor by one-third from the quality factor when the feedback controller was off. This evaluation system enabled the investigation of the performance of the MEMS active vibration isolator in a low pressure environment. This is important since many applications would require its use in a hermetically sealed package at low pressure.

The MEMS evaluation system was useful for investigating the MEMS relative velocity sensor's output response at low pressure. This was important because it is a key part of the active vibration isolator. Previously, the results showed that the displacement in low pressure was greater than the displacement at ambient pressure, where the MEMS structure had a lower quality factor.

The damping effect in various gases at different pressures was investigated in the MEMS evaluation system. It was observed that the density of the gas was more critical than the viscosity. As the pressure decreased, the damping also decreased, which was detected by observing changes in the device's quality factor from the recorded transmissibility plots.

The evaluation system was also used to investigate the effects on capacitance in various gases at various pressures. Since the force produced by MEMS electrostatic actuators is proportional to capacitance, this test was performed to see if the performance of these actuators could be enhanced by optimizing the surrounding gas chemistry and pressure. A comparison with absolute capacitance values was meaningless due to a large discrepancy in probe calibration of the LCR meter. The measured capacitance decreased as the pressure and permittivity of the gas under investigation decreased, except for air. It is believed that this was due to moisture in the air used during the test. The moisture resulted in higher measurements than would be expected with dry air. Furthermore, it is speculated that as the pressure was lowered, water molecules were liberated from surfaces in the vacuum chamber, which would keep the measured capacitance values higher than expected, due to the high dielectric constant of water vapor. It is also speculated that the ”pure” gases evaluated in the system may not have had the same interaction with water molecules in the vacuum system, thereby occluding their effect on the overall capacitance measurements.

In summary, the primary accomplishment of this endeavor was the development of an evaluation system for unpackaged MEMS die that allowed both electrical and mechanical characterization. Furthermore, this system allowed the evaluation to be performed in various gas chemistries at pressures lower than ambient air pressure. This system was then used to evaluate several MEMS devices and integrated microsystems.

CHAPTER 7

FUTURE WORK

The current MEMS evaluation system does not have the capability to control vaporization of water at very low pressure inside the bell jar chamber for evaluating the effects of high concentrations of water vapor at low pressures. This could be useful due to the high dielectric constant of water vapor. Attempts to control the water vaporization were not successful with a Thermal Electric Cooler (TEC). If a TEC with more power capacity is used, and a hygrometer is added, water vapor control could possibly be achieved at a low pressure for a more accurate evaluation.

The leak rate of the vacuum chamber was observed to be approximately 0.007 Torr/min. This can affect the gas environment inside the vacuum chamber during the test by adding moisture as well as air into the chamber. Therefore decreasing the leak rate would improve the evaluation system.

Thermal testing using the built-in heater was not performed under this research effort. Evaluating the viscosity of various gas chemistries over pressure and temperature would be useful. Other evaluation tools could be added to the system to enhance its capabilities. Examples could include a rotating stage for MEMS gyroscope testing, a residual gas analyzer (RGA), and an embedded optical camera with magnification optics. An integrated miniature probe station would enhance the evaluation of bare die without having to use machined fixtures to hold the die.

BIBLIOGRAPHY

[1] Jeff LaFrenz, Giorgio Grattiker, Karan V.I.S. Kaler, Martin P. Mintchev, "Starting from Scratch: Creating an Information Technology Infrastructure for MEMS-related Research and Development," International Journal " Information and Communication Technologies and Programming," 2003, pp. 12-21.

[2] Chi-Yuan Lee, Guan-Wei Wu, Wei-jung Hsieh, "Fabrication of micro sensors on a flexible substrate," Sensors and Actuators A 147 (2008) pp. 173-176.

[3] A. Nisar, Nitin Afzulpurkar, Banchong Mahaisavariya, Adisorn Tuantranont, "MEMS-based micropump in drug delivery and biomedical applications," Sensors and Actuators B 130 (2008) pp. 917-942.

[4] A. K. Poddar, K. N. Pandey, "Microwave Switch Using MEMS-technology," Sensors and Actuators A 147 (2008) pp. 173-176.

[5] S. Hurlebaus, L. Gaul, "Smart structure dynamics," Mechanical Systems and Signal Procesisign 20 (2006) pp. 255-281.

[6] Gregory T. A. Kovacs, NADIM I. Maluf, and Kurt E. Petersen, "Bulk Micromachining of Silicon," Proceedings of The IEEE, Vol. 86, No. 8, August 1998 pp. 1536-1551.

[7] James M. Bustillo, Roger T. Howe, and Richard S. Muller, "Surface Micromachining for Microelectromechanical Systems," Proceedings of The IEEE, Vol. 86, No. 8, August 1998 pp. 1552-1574.

[8] Yunn-Shiuan Liao, Shiang-Woei Chyuan, and Jeng-Tzong Chen, "FEM versus BEM," IEEE Circuits & Devices Magazine, September/October 2004 pp. 25-34.

[9] M.H. Zaman, S.F. Bart, J.R. Gillbert, N.R. Swart, and M. Mariappan, "An Environment for Design and Modeling of Electromechanical Micro-systems," JMSM, Vol. 1, No. 1, 1999 pp. 65-76.

[10] Software: http://www.coventor.com/mems/analyzer/index.html, CoventorWare

[11] Software: http://intellisensesoftware.com/Solutions/Solutions.html, IntelliSuite.

[12] Software: http://www.softmems.com/products.html, MEMS Pro/MEMS Xplorer

[13] D.J. Combes, K.M. Brunson and R. J. T. Bunyan, "Dynamic Simulation of MEMS Switches Using Simulink," Nanotech, Vol. 2, 2003 pp. 456-459.

[14] Software: http://www.mathworks.com/products/simulink/?BB=1, Matlab, Simulation

[15] Abhijeet Kolpekwar, R. D. Blanton, "Development of a MEMS Testing Methodology," International Test Conference, IEEE, 1997 pp. 923-931.

[16] Gino Rinaldi, Muthukumaran Packirisamy, Ion Stiharu, "Dynamic Testing of Micromechanical Structures under thermo-electro-mechanical Influences," ScienceDirect, Measurement 40, 2007, pp. 563-574.

[17] V. T. Srikar, S. M. Spearing, "A Critical Review of Microscale Mechanical Testing Methods Used in the Design of Microelectromechanical Systems," Society for Experimental Mechanics, Vol. 43, No. 3, September 2003 pp. 238-247.

[18] http://www.polytec.com/usa/_files/LM_AN_INFO_0103_E_Vibrometry_Basics.pdf, Measurement Solutions

[19] Christian Rembe, Richard S. Muller, "Measurement System for Full Three-Dimensional Motion Characterization of MEMS," IEEE, Journal of Microelectromechanical Systems, Vol. 11, No. 5, October 2002 pp. 479-488.

[20] R. M. Lin, W. J. Wang, "Structural dynamics of microsystems - current state of research and future directions," ScienceDirect, Mechanical Systems and Signal Processing 20 (2006) pp. 1015-1043.

[21] Dennis M. Freeman, C. Quentin Davis, "Using Video Microscopy to Characterize micromechanical Systems," IEEE/LEOS Summer Topical Meetings, 1998 pp. 9-10.

[22] http://umech.mit.edu/people/freeman/freeman_mems/

[23] C. Rembe, B. Tibken, E. P. Hofer, "Analysis of the dynamics in microactuators using high-speed cine photography," IEEE Journal of Microelectromechanical Systems 10 (2001) pp. 137-145.

[24] http://www.suss.com/products/test_systems/jp/test_systems, PAP200

[25] http://www.emopto.com/, Model 622-A 3-D MEMS Profiling System

[26] Benoît Charlot, Salvador Mir, Fabien Parrain, and Bernard Courtois, "Electrically Induced Stimuli For MEMS Self-Test," IEEE 2001 pp. 210-215.

[27] S. Mir, L. Rufer, A. Dhayni, "Built-in-self-test techniques for MEMS," Microelectronics Journal 37 (2006), pp. 1591-1597.

[28] Xingguo Xiong, Yu-Liang Wu, and wen-Ben Jone, "A Dual-Mode Built-in Self-Test technique for Capacitive MEMS Devices," IEEE Transaction on instrumentation and measurement, Vol. 54, No. 5, October 2005 pp. 1739-1750.

[29] Stephen Beeby, Graham Ensell, Michael Kraft, Neil White, " MEMS Mechanical Sensors," Artech House, Inc, Chapter 5, pp. 104-105.

[30] Harald Sehr, Alan G R Evans, Arthur Brunnschweiler, Graham J Ensell, and Trevor E G Niblock, "Fabrication and test of thermal vertical bimorph actuators for movement in the wafer plane," Journal of Micromechanics and Microengineering, 11 (2001), pp. 306-310.

[31] Ankur Jain, Hongwei Qu, Shane Todd, Huikai Xie, "A thermal bimorph micromirror with large bi-directional and vertical actuation," Sensors and Actuators, A 122 (2005), pp. 9-15.

[32] Sergey Edward Lyshevshi, " MEMS and NEMS Systems, Devices, and Structures," CRC Press, Chapter 2, p. 51.

[33] Chia-Yen Lee, Hsien-Tsung Chang, and Chih-Yung Wen, "A MEMS-based valveless impedance pump utilizing electromagnetic actuation," Journal of Micromechanics and Microengineering, 18 (2008), pp. 35-44.

[34] Sangkyung Sung, Jang Gyu Lee, Byeungleul Lee, and Taesam Kang, "design and performance test of an oscillation loop for a MEMS resonant accelerometer," Journal of Micromechanics and Microengineering, 13 (2003), pp. 246-253.

[35] Robert Neal Dean, Jr., George T. Flowers, Roland Horvath, Nicole Sanders, A. Scottedward Hodel, John Y. Hung, Thaddeus Roppel, "Characterization and Experimental Verification of the Nonlinear Distortion in a Technique for Measuring the Relative Velocity Between Micromachined Structures in Normal Translational Motion," IEEE Sensors Journal, Vol. 7, No. 4, April 2007 pp. 496-501.

[36] http://www.lds-group.com/docs/display_product.php?product_item_id=442, Model V830 Electrodynamic Shaker, LDS

[37] Ashwin Mohan, Ajay P. Malshe, Shyan Aravamudhan, and Shekhar Bhansali "Piezoresistive MEMS Pressure Sensor and Packaging for Harsh Oceanic Environment," IEEE Electronic Components and technology Conference, 2004 pp. 948-950.

[38] Keith B Brown, Walter Allegretto, Fred E Vermeulen and Alexander M Robinson, "Simple resonating microstructures for gas pressure measurement." Journal of Micromechanics and Microengineering, 12 (2002), pp. 204-210.

[39] R.N. Dean, G.T. Flowers, A.S. Hodel, G. Roth, S. Castro, R. Zhou, A. Moreira, A. Ahmed, R. Rifki, B.E. Grantham, D. Bittle and J. Brunsch, "On the Degradation of MEMS Gyroscope Performance in the Presence of High Power Acoustic Noise," Proc. of the 2007 IEEE Int. Symposium on Industrial Electronics (ISIE 2007), Vigo, Spain, June 4-7, 2007, pp. 1435-1440.

[40] http://www.polytec.com/usa/158_379.asp, LSV 6000 Surface Velocimetry Optical Profiler

[41] http://www.polytec.com/usa/158_426.asp, MSA-500 Micro System Analyzer

[42] http://www.veeco.com/pdfs/datasheets/ds525 20dmems 20data 20sheet_396,pdf, Wyko NT1100 Dynamic MEMS Measurement System

[43] http://www.suss.com/products/test systems/jp/test systems, SUSS PAP200 Pressure Sensor Tester

[44] http://www.polytec.com/usa/158 426.asp, Polytec MSA-400 Microscope Scanning Vibrometer

[45] S.J. Kim, C. Chen, G. Flowers and R. Dean, ”Active damping control of micromachined devices in a low atmospheric pressure environment,” Proc. of SPIE Smart Structures and Materials & Nondestructive Evaluation and Health Monitoring 2008, Vol. 6928, San Diego, CA, March 9-13, 2008 (11pp).

[46] Seong Jin Kim, Chen Chen, Robert Dean, George Flowers, A. Scottedward Hodel, Stanley J. Reeves, “A Packaging Solution to Reduce Electrical Noise in MEMS Capacitive Elements Resulting from Environmental Mechanical Vibration,” IMAPS 4th International Conference on Device Packaging, AZ, March 2008.

[47] ROBERT N. DEAN, “A Technique for the Measurement of Relative Velocity between Parallel Plate Electrodes in Micromachined Structures”, Auburn University Graduate School, 5/11/2006.

[48] David R. Lide, “Handbook of Chemistry and Physics,” 84^{th} Edition, 2003-2004, CRC Press

[49] N. Ernest Dorsey, “Properties of ordinary water-substance,” No81 ReinHold Publishing Corp., 1940.

[50] http://www.analog.com/en/mems-and-sensors/imems-accelerometers/adxl180/products/product.html

APENDICES

APPENDIX A

A.1 Micromachined Si MEMS Device Fabrication Procedure

I. 350μm DSP Si Wafer Clean

1. 50:1 H_2O:HF at ambient for 30s
2. 6:1:1 H_20:HCL:H_20_2 at 80°C for 10min
3. DI water rinse and blow dry

II. Dehydration

1. 20min at 120°C in dehydration oven

III. Top Side Photolithography

1. 3min O_2 clean in Matrix
2. 15min vapor phase HMDS deposition at ambient
3. PR spin: Clarient 5214E, 1000RPM, 30s
4. Softbake: 108°C for 2min on hotplate
5. Soak glass plate in cooled (after 10min) piranha etchant for 2min
6. DI water rinse and N blow dry glass plate
7. Mount ”Pas Top 11/12/04” photoplot on glass plate with tape
8. MABA6: 14s exposure with photoplot attached to glass plate mask
9. Develop: Clarient AZ 400K, 2:1, 30s

10. DI water rinse and blow dry

IV. Top Side DRIE

1. 40μm Si etch in STS ASE
2. Inspect often
3. As close to 40um as possible

V. Top Side Photoresist Strip

1. 5min O_2 clean in Matrix (500W, 5Torr)

VI. Bottom Side Photolithography

1. 3min O_2 clean in Matrix
2. 15min vapor phase HMDS deposition at ambient
3. PR spin: 1045, 1000RPM, 30s
4. Softbake: 108°C for 2min on hotplate
5. Soak glass plate in cooled (after 10min) piranha for 2min
6. DI water rinse and N blow dry glass plate
7. Mount ”Pas Bot 11/12/04” photoplot on glass plate with tape
8. MABA6: 60s exposure with photoplot attached to glass plate mask
9. Develop: Clarient AZ 400K, 2:1, 30s+ (until fully developed)
10. DI water rinse and blow dry
11. Hardbake: 120°C for 2min on hotplate
12. DI water rinse and blow dry

VII. Bottom Side DRIE 1

   1. 140μm Si etch in STS ASE

VIII. Cleave Wafer

   1. Using a diamond cutter, the etched lines parallel to the flat edge of the wafer are extended to each end of the wafer. The wafer is then aligned in a clamp and carefully snapped at each horizontal cut. This snapping is then repeated for the perpendicular etched lines.

IX. Oxidize Test Wafer

   1. Push in at 900°C
   2. Ramp to 1050°C
   3. N_2 - 5 minutes
   4. O_2 - 5 minutes
   5. O_2, H_2 - 1 hour
   6. O_2 - 5 minutes
   7. N_2 - 5 minutes
   8. Ramp down to 900°C and pull out

X. Die Mount 1

   1. PR spin: 4620, 2000 rpm, 700 ramp, 30s
   2. Place four die symmetrically on the test wafer with bottom side up and gently apply pressure onto each die.
   3. Softbake: 108°C for 3min on hotplate

XI. Bottom Side DRIE 2

1. 170μm Si etch in STS ASE
2. Etch until part released - check if the top and bottom etching side meet each other under the microscope; if they meet, the color turned to red or black. If not, check it after every cycle: rotate the wafer by 90° every cycle.
3. Check often to prevent over etching

XII. Post DRIE MEMS Die Removal

1. Prepare two glass dishes and pour the acetone. Cut the wiper tissue and put it into each dishes; this tissue will be used for moving the die from the dishes not to break them.
2. Soak the wafer for 30 to 60 min.
3. Gently stir the dish and check if each die are away from the wafer. If not, wait more. Repeat it every 15min.
4. Move the wafer and die using the wiper tissue. Gently remove each die and move them to another dish to clean.
5. Prepare a glass dish and pour the isopropyl alcohol. Rinse1: Move the die and put them into the the isopropyl alcohol using the wiper tissue.
6. Rinse2: Move them out of the dish using the wiper tissue. Change the alcohol to a new one and put them into it again using the wiper tissue.
7. Soak MEMS die in DI water bath using the wiper tissue.
8. Allow MEMS die to air dry in a very soft blow.
9. Rinse test wafer in DI water and N blow dry.

XIII. Post DRIE Clean

1. Place MEMS die on holder wafer, bottom side up.
2. 5min O_2 clean in Matrix (500W, 5Torr) [until all photoresist removed]
3. Place MEMS die on holder wafer, top side up.
4. 5min O_2 clean in Matrix (500W, 5Torr) [until all photoresist removed]

XIV. E-Beam Metallization

1. Mount die onto a holder wafer with top side up. Die are held down with a narrow piece of Kapton tape on each corner.
2. 2min Ar ion clean
3. 800A Ti - E-beam
4. 2000A Au - E-beam
5. CAREFULLY remove blue tape from corners of MEMS die (The edges of the tape are carefully pealed up from the wafer, but left on the die. Once all the edges have been removed, and the die can be lifted from the wafer, the tape can be fully removed from the die.)
6. Inspect MEMS die

A.2 How To Use the Evaluation System

This section explains how to use the MEMS evaluation system to test MEMS devices.

1. Locating the small shaker

    - The shaker is located on top of the graphite heating plate. Make sure that the heating plate is securely mounted over heating lamp and put the shaker on the even heating plate. Once the shaker is located on the plate, the shaker's power cable should be connected through the electrical feedthrough to the shaker. Then, DUT article can then be attached to the shaker head.

2. Cable Setup Between Equipment

    - The Nine Connection wires between Inside and Outside: Inside and outside the bell jar, there are nine electrical connections passing through the 9-D sub electrical connector in the electrical feedthrough. Among the nine connection wires, two lines are used for the shaker power cable, which is a very thin coaxial cable connecting to the shaker. For the applications under this endeavor, four connections are used not only to provide an electronic circuit board with +/-25V power and ground but also to receive the output signal of the capacitor voltage from the board. The rest of the three connection wires are reserved for additional purpose. For example, if a TEC peltier and a thermistor are installed inside the chamber to control the water vaporization, four more wires would be needed. So, three reserved wires and one wire among the used ones need to connect to them. Nine connection wires are connected to the external cable through the electrical feedthrough. Under this endeavor, the nine electrical wires from the 9-pin D-sub connector are used to connect to a power supply, a LCR meter and/or an oscilloscope.

- Cables between Laser Interferometer Controller and Signal Analyzer: The coaxial cable is connected between the BNC port of the interferometer controller and one of two input channel ports of the signal analyzer. The output from the interferometer controller measuring the displacement of MEMS outer frame should be connected to channel 1 port of the signal analyzer.
- Cables between Shaker Power Amplifier and Small Shaker: The small shaker needs to receive power from the shaker amplifier, so the power line from the red and black ports are connected to the small shaker through the 9-pin D-sub connector. A BNC line port in the small shaker, which receives the control signal, is connected to two line from the 9-pin D-sub connector inside. (Refer to Figure A.1)
- Cables between Shaker Power Amplifier and Signal Analyzer: A BNC output port of signal analyzer is connected to the input port of the shaker power amplifier by using a coaxial wire. (Refer to Figure A.1)

3. Dynamic Signal Analyzer Setup

   - Measuring the Mechanical Frequency Response: To measure the mechanical frequency response, the analyzer should be set to FFT mode for two channels. Then, set it to the dual display mode and Hamming mode. Adjust the input frequency range, source level, and input wave type. (400Hz to 3600 Hz, 70 to 100 mVrms, and random signal are the parameters used for transmissibility testing for this endeavor). Once the resonant frequency is detected, while shaking the MDUT with a sine wave input at the resonant frequency, time traces of the velocity direction are recorded. Especially, in order to get

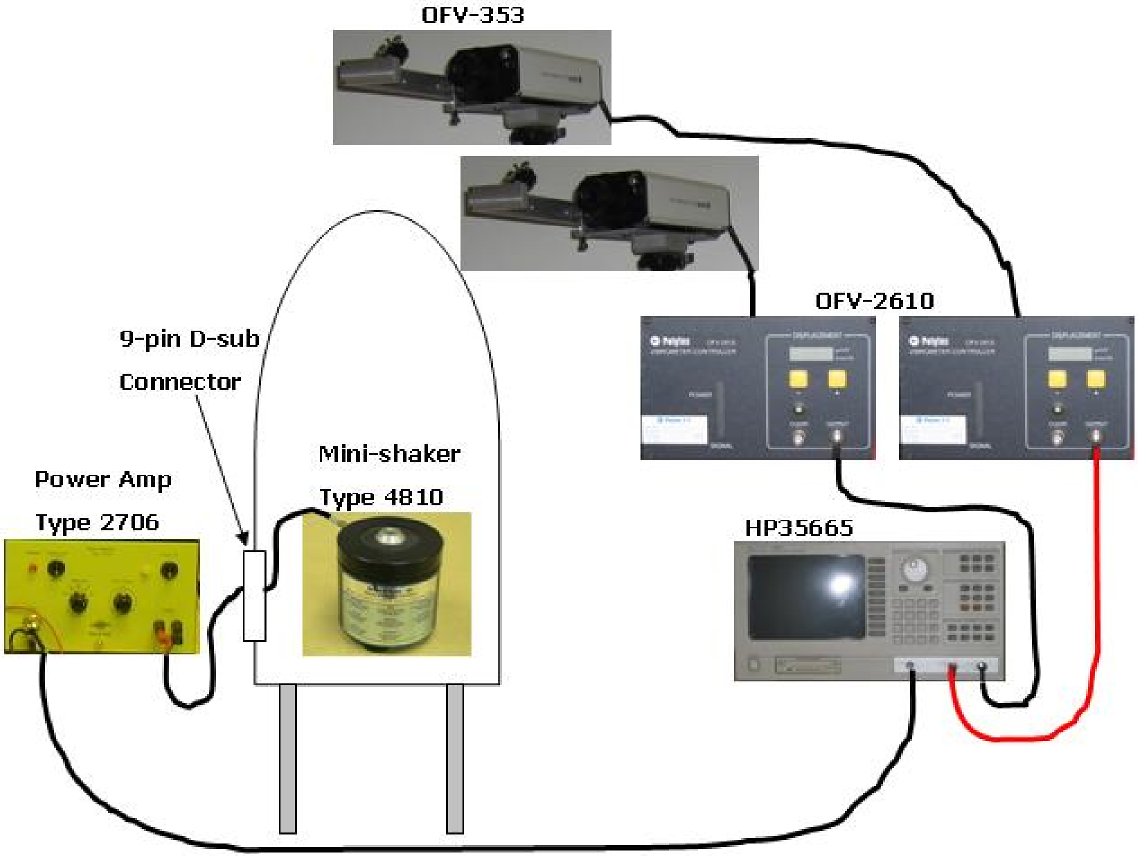

Figure A.1: Cable Connection between Equipment a clean output result, change unit of μm/V in the laser controller until noise in the output wave disappears.

4. Laser Controller Setup

   - The laser controller has a range of 20μm/V to 5120μm/V unit. Depending on the output signal level, a suitable unit needs to be set for a clean output result.

5. Focusing the Laser Spot of the Interferometer

   - For a test in ambient pressure, the glass bell jar is not used. Therefore, the laser beam directly reflects from the surface of MDUT, and the signal strength is over 90%. For a low pressure test, the chamber is covered with the glass bell jar, which leads to difficulties in focusing and obtaining a high signal strength due to the refraction by the curved surface of the bell jar. Move the laser beam position and adjust the mirror until over 90% of the signal strength can be received.

6. Gas Handling Valves

   - Please refer to the valve pluming configuration diagram in Figure 4.8. The N_2 valve and SO_2 gas valve are located in a metal cabinet at the back of the yellow room. The N_2 is used for purging as well as an evaluation gas. To supply the N_2 and SO_2 (or other gases) to the chamber, the valve in the cabinet needs to be open or closed. In the case of SF_6 gas, the gas cylinder in its cart is connected to the Tee of the flow meter, which has the main ball valve and precise control valve. These three valves including a valve of the SF_6 gas cylinder are used to open or close for supplying the SF_6.

7. Pumping Down the Chamber

- To pump down the chamber, the main ball valve and precise valve are closed and the bellows valve is opened. The analog pressure gauge is used over the range of 760 Torr to 1 Torr, and for lower pressures (less than 1 Torr), the digital, digital readout displays accurate pressure reading. The minimum pressure obtainable in the current system is 50 mTorr. It takes around four hours to reach at 50 mTorr and less than 15 minutes to reach at 1 Torr. If it takes longer, the operator should check for leaks in the system.

8. Pumping Up the Chamber

   - The N_2 is injected into the chamber while the bellows valve is closed and the precise valve is open slightly, so that the bell jar cover does not pop up due to the high pressure of the N_2. While watching the pressure gauge and the flow meter, the precise valve should be used to regulate the gas flow.

9. Maintaining a Certain Pressure

   - Maintaining a certain pressure is not easy due to leaks in the system. By adjusting the bellows valve precisely with the two inlet valves closed, equilibrium status between pumping down and air injection can usually be accomplished.

10. Controlling the N_2 and SO_2 Gas Valves in the Pump Room

    - As presented in Figure 4.9, the main valve should be open to supply SO_2 gas. Then, a proper pressure can be adjusted with the regulator valve of the SO_2 cylinder. N_2 gas can be supplied by opening the N_2 main valve and then the N_2 control valve. The N_2 check valve allows the operator to determine if there is N_2 gas in the tank. In order to stop supplying a gas, the main valves for each gas are closed.

11. Purging a Gas

    - After a toxic gas such as SO_2 is used for a test, valves of the SO2 and N2 gases are closed. Then the bellows valve is opened to vent the residual SO_2 gas from the plumbing and the chamber for a few minutes. Then N_2 gas valve is opened to inject N2 gas into the plumbing line and the chamber. The N_2 gas valve should not be opened fully when the bellows valve is open, to avoid overconsumption of N_2 gas. The operator can also adjust the N2 gas flow using the precise valve, even when the N_2 valve is fully open.

12. The Order of Turning on Equipment

    - Once all the cables are connected, as explained in the cable setup section, turn on the equipment in the following order. Vibrometer controller → laser unit → (signal analyzer → set all the parameter of the signal analyzer) → (the small shaker power amplifier → increase the amplification by rotating the adjustment knob to the designated line), When turning off the equipment, do this procedure in the reverse order. NOTE: if the signal analyzer is off with the shaker power amplifier is on, the shaker can be damaged due to the peak surge from the analyzer.